11

B-site Multi-element Doping Effect on Electrical Property of Bismuth Titanate Ceramics

Jungang Hou[1] and R. V. Kumar[2]
[1]*School of Metallurgical and Ecological Engineering, University of Science and Technology*
[2]*Department of Materials Science and Metallurgy, University of Cambridge*
[1]*China*
[2]*United Kingdom*

1. Introduction

This article represents a systematic review of the behaviour of B-site multi-element doping effect on electrical property of bismuth titanate ceramics. Bismuth titanate, $Bi_4Ti_3O_{12}$ (BIT) is a potential candidate for high-temperature device applications due to their high dielectric constant, Curie temperature (T_c), breakdown strength, anisotropy and, low dielectric dissipation factor, therefore attracting considerable commercial interest in applications such as high temperature piezoelectric devices, memory storage and optical displays. These features make bismuth layer-structured ferroelectrics (BLSFs) attractive in the field of developing lead-free piezoelectric materials. BIT is a well-known member of the BLSFs, which can be represented by a general formula $(Bi_2O_2)^{2+}(A_{m-1}B_mO_{3m+1})^{2-}$, where A represents a mono-, di, or trivalent ion, such as La^{3+}, Nd^{3+}, Pr^{3+}, Sm^{3+}, etc., B stands for transition-metal cations like Ti^{4+}, Nb^{5+}, Ta^{5+}, W^{6+}, etc., and m is the number of BO_6 octahedra in the perovskite-like layer (m=1-5) (Aurivillius, 1949; Kumar, 2001; Markovec, 2001; Nagata, 1999; Noguchi, 2000; Sugibuchi, 1975; Shimakawa, 2000; Subbarao, 1961; Shulman, 2000; Shimazu, 1980l; Takenaka, 1981). The layer structure of $Bi_4Ti_3O_{12}$ (m=3) consists of three perovskite-like $(Bi_2Ti_2O_{10})^{2-}$ units with a pseudo-perovskite layer structure, sandwiched between $(Bi_2O_2)^{2+}$ layers along its crystallographic c axis. In the $(Bi_2Ti_2O_{10})^{2-}$ units, Ti ions are enclosed by oxygen octahedra, and Bi ions occupy the spaces in the framework of octahedral (Subbarao, 1950).

BIT is of interest in high-temperature piezoelectric sensors, because it remains ferroelectric up to 675 °C and offers relatively high piezoelectric property (Subbarao, 1961). However, the high leakage current and domain pinning due to defects in BIT have appeared as obstacles for further applications. The reasons for such problems are suggested due to the instability in the oxidation state of Ti ions and the volatile property of Bi during the sintering process (Nagata, 1999). Great efforts have been made to solve the high-leakage current, by incorporation of W, Nb or Ta dopants, as these can significantly decrease the conductivity in BIT (Hong, 2000; Markovec, 2001; Shulman, 1999; Takenaka, 1981; Villegas, 1999; Zhang, 2004). Unfortunately, the piezoelectric effect in the high Curie temperature BIT is relatively low, with coefficient values typically less than 20 pC N^{-1} found for both pure and modified $Bi_4Ti_3O_{12}$. Thus, it is a challenge to seek a rational pathway to improve the electrical property of BIT ceramics.

We have reported in our publications, the effects of composition and crystal lattice structure upon microstructure, dielectric, piezoelectric and electrical properties of BIT, $Bi_4Ti_{3-x}W_xO_{12+x}$+0.2wt%Cr_2O_3 (BTWC), $Bi_4Ti_{3-2x}Nb_xTa_xO_{12}$ (BTNT) and $Bi_4Ti_{3-2x}Nb_xTa_{x-y}Sb_yO_{12}$ (BTNTS) ceramics have been widely investigated (Hou et al, 2009, 2010 and 2011). The processing of as-synthesized BIT were optimized and the main parameters were determined, and confirmed that the piezoelectric coefficient (d_{33}) of undoped BIT is 8 pC N^{-1}. As for BTWC, the results have shown the systematic changes in the lattice parameters; the formation of secondary phase(s) at higher levels of W/Cr doping; and the increase in dielectric constant and loss at room temperature with increase of doping content. A higher value of d_{33}, at 22 pC N^{-1}, was obtained for the sample with x=0.025, which may result directly from lowering conductivity. With regard to BTNT and BTNTS, the results have shown the formation of orthorhombic structure for all the samples within these family of dopants; the addition of Nb/Ta caused a remarkably suppressed grain growth while there is not much difference in grain size for BTNTS; as the doping content was increased, the Curie temperatures of BTNT decreased significantly, to as low as 630^{o}C while the difference is not very significant for BTNTS. The co-doping at B-site could induce the distortion of oxygen octahedral and reduce the oxygen vacancy concentration, resulting in the enhancement of d_{33}. Especially, the highest values of 26 and 35pC N^{-1}, were obtained for $Bi_4Ti_{2.98}Nb_{0.01}Ta_{0.01}O_{12}$ and $Bi_4Ti_{2.98}Nb_{0.01}Ta_{0.002}Sb_{0.008}O_{12}$, respectively. The activation energy associated with the electrical relaxation and DC conductivity were determined from the electric modulus spectra, suggesting the movements of oxygen ions are possible for both ionic conductivity as well as the relaxation process. To ascertain the electrical conduction mechanism in the ceramics, various physical models have been proposed, suggesting the conductivity behavior of the ceramics can be explained using correlated barrier hopping model. All measurements demonstrated that BTNT ceramics are promising candidates for high temperature applications.

2. W/Cr modified $Bi_4Ti_3O_{12}$ ceramics

Bismuth titanate, $Bi_4Ti_3O_{12}$ (BIT) is a potential candidate for high-temperature device applications due to their high Curie temperature (T_c) and an excellent fatigue endurance property. However, the piezoelectricity of pure BIT ceramics is relatively very low (d_{33} < 8 pC N^{-1}). The piezoelectric properties can be enhanced by grain orientation techniques. However these methods are not cost effective. So, it is favourable to optimize piezoelectric properties via structural modification using appropriate doping. In this connection, to improve the piezoelectric properties of BIT, ions substitution with other cations have been considered and explored. It has been shown that doping with donor cations such as Nb^{5+}, V^{5+} or Ta^{5+} in the Ti^{4+} positions decreases electrical conductivity and improves piezoelectric properties of BIT ceramics (Du, 2009; Shulman, 1999; Tang, 2007). Cr doping is another one of the most adopted strategies to tailor the dielectric and piezoelectric properties of ferroelectrics to practical specifications. It is well known that Cr is effective in decreasing the aging effect and decreasing dielectric loss thus the effect of doping of Cr^{3+} is that of stabilizer of piezoelectric and dielectric properties (Li, 2008; Yang, 2007). The density of ceramics can be increased using small amount of Cr_2O_3. However, large content of Cr_2O_3 will inhibit grain growth because of accumulation of Cr^{3+} at the grain boundary, which results in decrease in the grain size (Hou et al, 2005; Takahashi, 1970).

It is noted that the studies concerning the effect of W^{+6} doping on electrical and sintering behavior have been reported earlier (Jardiel, 2006, 2008; Villegas, 2004). However reports on W/Cr doped BIT ceramics are scarce. We have made an attempt to optimize the W/Cr doping to yield enhanced piezoelectric and dielectric properties of BIT ceramics. The influence of W/Cr doping on the structural, sintering behavior, dielectric, electrical conductivity and piezoelectric properties of BIT ceramics is reported in this section.

Fig. 1 (A) shows the X-ray diffraction patterns of BITWC ceramics at room temperature. Diffraction data does not show any evidence of the formation of tungsten and chromium oxide or associated compounds that contain bismuth or titanium. Therefore, the BITWC ceramics maintains a layer structure similar to the perovskite BIT even under extensive modifications by W^{6+}/Cr^{3+}.

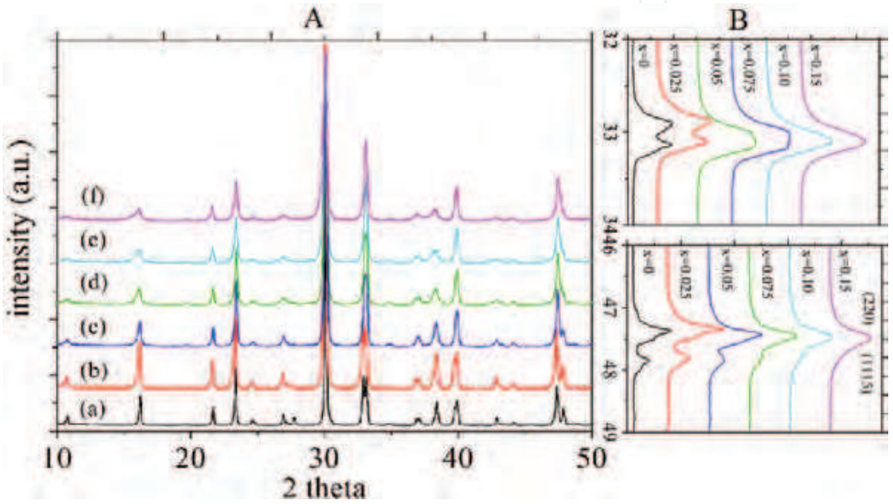

Fig. 1. (A) XRD patterns of BITWC with different W/Cr content: (a) 0.0, (b) 0.025, (c) 0.05, (d) 0.075, (e) 0.10 and (f) 0.15. (B)Evolution of XRD patterns associated with the peaks of (020)/(200) and (220)/(1115) of BITWC powders with different W/Cr content.

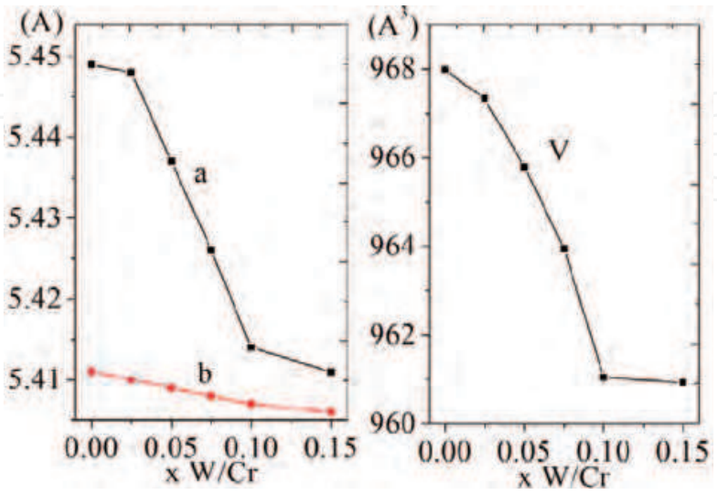

Fig. 2. Variation in lattice parameters of BITWC powders calcined at 800 °C for 4 h vs. different amount of W/Cr doping.

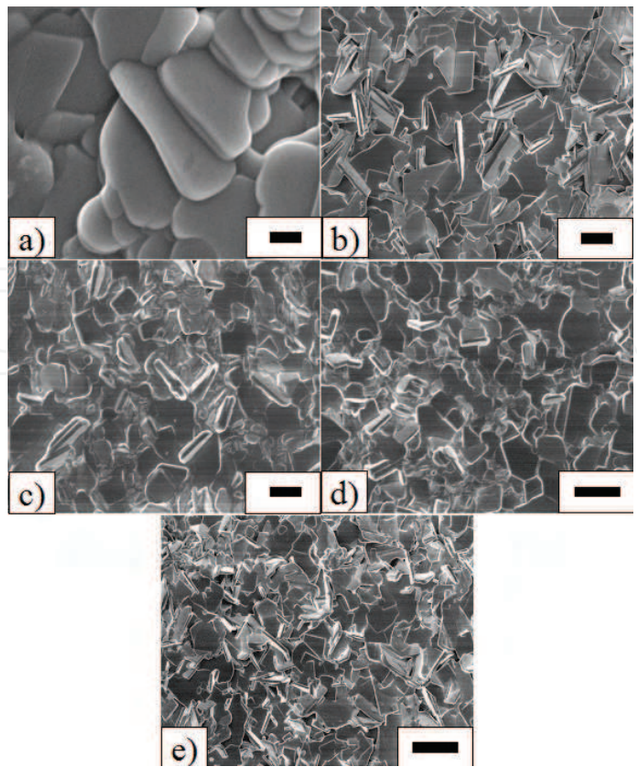

Fig. 3. SEM images of polished and thermal etched surfaces of various samples: (a) 0.025, (b) 0.05, (c) 0.075, (d) 0.10 and (e) 0.15. Scale represented in the figures is 3 μm.

Evolution of XRD patterns associated with the peaks of (020)/(200) and (220)/(1115) of BITWC with different W/Cr content are shown in Fig. 1 (B). For sample with 0.025W/Cr, the (020) diffraction pattern at 2θ=33° is clearly split into two (020) and (200) peaks in the orthorhombic phase thus the lattice constants $a \neq b$. With increasing W/Cr content, the splitting between the (020) and (200) peaks is decreased, indicating the reduction of the orthorhombicity a/b. When x=0.05, only the reflection (020) can be observed and the (020) reflections have shifted to higher 2θ values, indicating a decrease in the lattice parameters a and b in the crystal structure. From Fig. 1 (B) the (220) reflections are observed to shift upwards in the orthorhombic form and the reflection (1115) is absent at x=0.10. That means the modification of tungsten and chromium for titanium ions distorts the positions of ions in the lattice, which may result from the different lattice strain relating to different ionic radius and outer electronic configuration between W^{6+} and Cr^{3+}. As typically shown in Fig. 2, the decrease of the orthorhombic lattice parameters a and b, and lattice volume V of the BIT phase with an increasing amount of W/Cr doping are obvious, especially for the composition with W/Cr being less than 0.10. Further an increase in the amount of W/Cr to 0.15 does not cause a change of cell dimensions based on XRD results. However, no significant drop in lattice parameter, c, is found in BITWC powders calcined at 800 °C for 4 h. It is observed that the almost no volume change could be found for powders with W/Cr doping more than 0.10, allows us to further study the possibility of the formation of a second phase like $Bi_6Ti_3WO_{18}$ and $Bi_6Ti_5WO_{22}$ in the samples (Jardiel, 2008), although any secondary phases were not found by XRD techniques because of the limitation of XRD intensity below a certain concentration. A careful examination of the XRD patterns in Figs. 1

(B) reveal that apart from the decrease of the lattice parameters and the difference between the a and b parameters, the peaks have broadened. The (1115) peaks in the patterns of x=0.10 and 0.15 appear as a weak shoulder on the right of the corresponding (220) peaks. Although the line-broadening of XRD peaks can have various origins, including grain size and dislocation structure (Snyder, 1999), it is expected that the observed line-broadening can be attributed to micro -strain in the material.

Fig. 3 shows the SEM images of the polished and thermally etched surfaces of BITWC ceramics. It is observed that the average grain size decreased with W/Cr doping ranging from approximately 10 μm to 1 μm, which suggest that W/Cr control the growth of the plate-like grains. It is reported that WO_3 influences the grain growth kinetics due to the slowing of grain boundary diffusion processes (Jardiel, 2008). The aspect ratio of the grains decreases with increase of W/Cr doping as shown in Fig. 3. This will lead to a better arrangement of the particles during the sintering processes and consequently to an enhanced densification of the ceramics. Table I shows the EDS analysis data of BITWC ceramics. When $x \leq 0.05$, the experimentally observed atomic ratios agreed with the initial compositions signifies that the BITWC ceramics are single phase. This shows that the W^{6+}/Cr^{3+} cations were incorporated into the layered perovskite structure and presumably occupied Ti^{4+} sites. While for $x \geq 0.075$ compositions, EDS results were not in agreement with the initial theoretical atomic ratios. This indicates the presence of the secondary phases in the samples.

Element	BIT	x=0.025	x=0.05	x=0.075	x=0.1	x=0.15
Bi	4.00	3.98	3.97	3.96	3.93	3.87
Ti	2.99	2.98	2.94	2.91	2.86	2.81
W	0	0.025	0.05	0.076	0.11	0.16
Cr	0	0.4	0.4	0.39	0.4	0.37
O	12.00	12.00	12.00	12.08	12.09	12.16

Table 1. Energy-Dispersive Spectra (EDS) Analysis Data for BITWC ceramics

Fig. 4 (a) shows the variation of the real part of impedance (Z') with frequency at various temperatures for x = 0.025 composition. It is observed that the magnitude of Z' decreases with increase in both frequency as well as temperature, indicating an increase in ac conductivity with rise in temperature and frequency. The Z' values for all temperatures merge at high frequencies. Similar trends were observed for the other compositions which are not depicted in the Fig. 4. Fig. 4 (b) shows the normalized imaginary parts of impedance (Z''/Z''_{max}) as a function of frequency at the selected temperatures. The values of (Z''/Z''_{max}) are observed to shift to higher frequencies with increasing temperature consistent with temperature dependent electrical relaxation behavior. These observed relaxation processes for the studied samples could be attributed to the presence of defect/vacancies.

Relaxation processes in many electric, magnetic, mechanical and other systems are governed by the Kohlrausch-Williams-Watts (KWW) law (Williams, 1970),

$$\varphi(t) = \exp\left[-\left(t/\tau\right)^{\beta}\right] \quad (1)$$

where τ is the relaxation time and $0 < \beta \leq 1$ is the parameter which indicates the deviation from Debye-type relaxation. The dielectric behaviour of the present ceramics is rationalized by invoking modified KWW function suggested by Bergman (Bergman, 2000). The imaginary part of the electric modulus ($Z^{"}$) can be defined as:

$$\frac{Z^{"}}{Z^{"}_{\max}} = \frac{1}{(1-\beta)+\frac{\beta}{1+\beta}\left[\beta\left(f_{\max}/f\right)+\left(f/f_{\max}\right)^{\beta}\right]} \tag{2}$$

where $Z^{"}_{\max}$ is the peak value of the $Z^{"}$ and f_{max} is the corresponding frequency. Theoretical fit of Eq. 2 to the experimental data is shown in Fig. 4 (b) as the solid lines. It is seen that the experimental data are well fitted to this model except in the low frequency regime which may be due to electrode effect associated with the samples. From the fitting of $Z^{"}$ versus frequency plots, the value of β was determined and found to be temperature independent. The value of β is found to be 0.82±0.02 in the 400-600 °C temperature range. Eq. 2 can be fitted for other compositions under study which are not shown in Fig. 4.

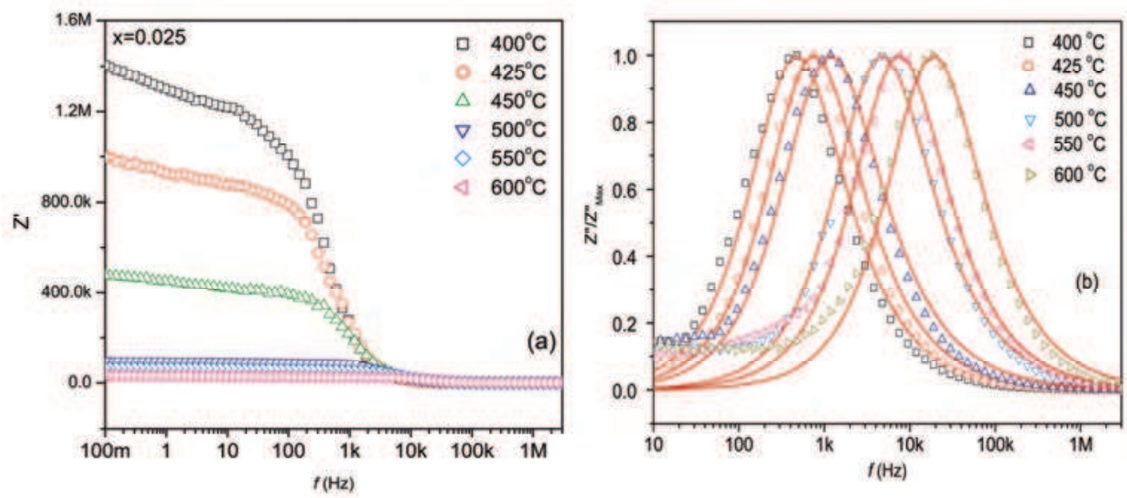

Fig. 4. (a) Real and (b) imaginary parts of impedance versus frequency plots at various temperatures and the solid lines are the theoretical fit.

Fig. 5 depicts the variation of relaxation frequency with an inverse of absolute temperature for the composition of x=0.025. The activation energy for electrical relaxation can be calculated using Arrhenius relation as:

$$f_m = f_o \exp\left(-E/kT\right) \tag{3}$$

where f_o is the pre exponential factor, k is the Boltzmann constant, and T is the absolute temperature. Activation energy was calculated from the linear fit of the experimental data as shown in Fig. 5 for x=0.025 samples. Activation energy was estimated for the other compositions under study and the plot for activation energy versus composition is shown in the inset of Fig. 5. The activation energy increases with the W/Cr content, which suggests a decrease of oxygen vacancy concentration (Coondoo, 2007).

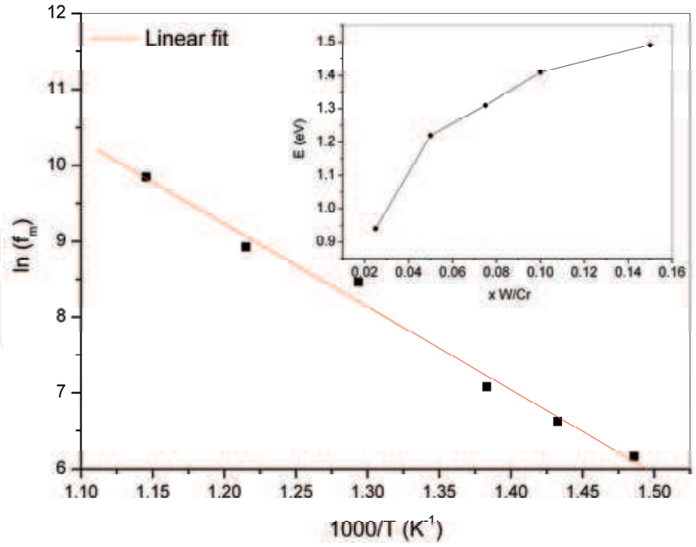

Fig. 5. Arrhenius plot for relaxation frequency versus temperature and inset shows variation of activation energy with x.

T (°C)	R_1 (ohm)	CPE (1) [nF]	n_1	R_2 (ohm)	CPE (2) [F]	n_2	R_3 (ohm)
450	1.98×10^5	1.26	0.88	1.14×10^5	3×10^{-6}	0.60	6333
500	5.7×10^4	1.8	0.89	3.3×10^4	2×10^{-5}	0.5	1300
550	2.2×10^4	1.66	0.89	1.5×10^4	1×10^{-5}	0.41	268
600	1.1×10^4	1.2	0.9	7871	0.037	0.35	0.01

Table 2. Cole-Cole fitted parameters for the x=0.025 samples

If we scale each Z'' with Z''_{max} and each f with f_{max}, the entire curves collapse into a single master curve as shown in the Fig. 6 for x=0.025 samples. The scaling nature of Z'' implies that the relaxation shows the same mechanism in the entire temperature range. Similar behaviors were also observed for the other compositions (x = 0.05, 0.075, 0.1 and 0.15) under study which are not shown here in the figure.

Figs. 7 depict complex impedance plots at 600 °C temperatures for x=0.025 samples. The complex impedance plots were resolved with two depressed semicircles corresponding to grain and grain boundaries. The impedance data for x=0.025 samples were fitted using superimposition of two Cole-Cole expressions as:

$$Z^* = \frac{R_1}{\left[1+(i\omega\tau_1)^{n1}\right]} + \frac{R_2}{\left[1+(i\omega\tau_2)^{n2}\right]} \tag{4}$$

where R_1, R_2, τ_1 and τ_2 are resistance and relaxation times from grain and grain boundaries, respectively. The factors n_1 and n_2 indicate poly-dispersive multi Debye type relaxation. If the values are unity then the relaxation is explained by Debye type response. Experimental data were fitted using the software "ZsimpWin" as shown in Fig 7(a-d). The electrical contribution of the grains and grain boundaries was introduced by using an equivalent circuit as shown in inset of Fig 7(a). The results show the well-fitted impedance plots to the

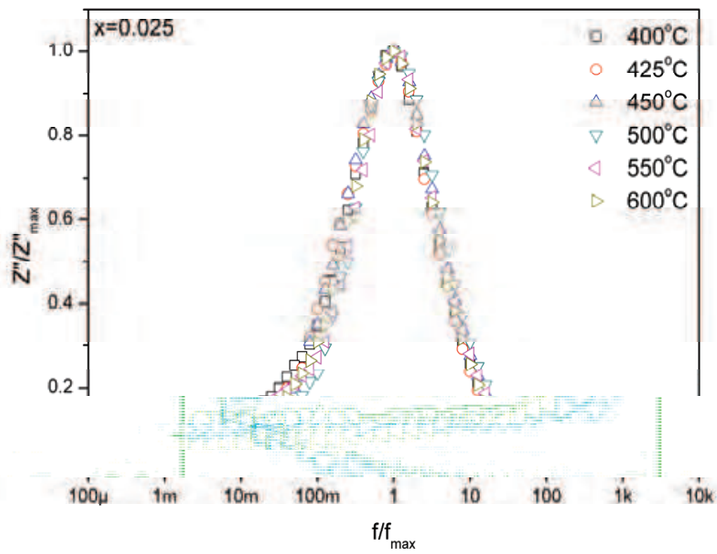

Fig. 6. Scaling behaviour of $Z^{''}$ at various temperatures.

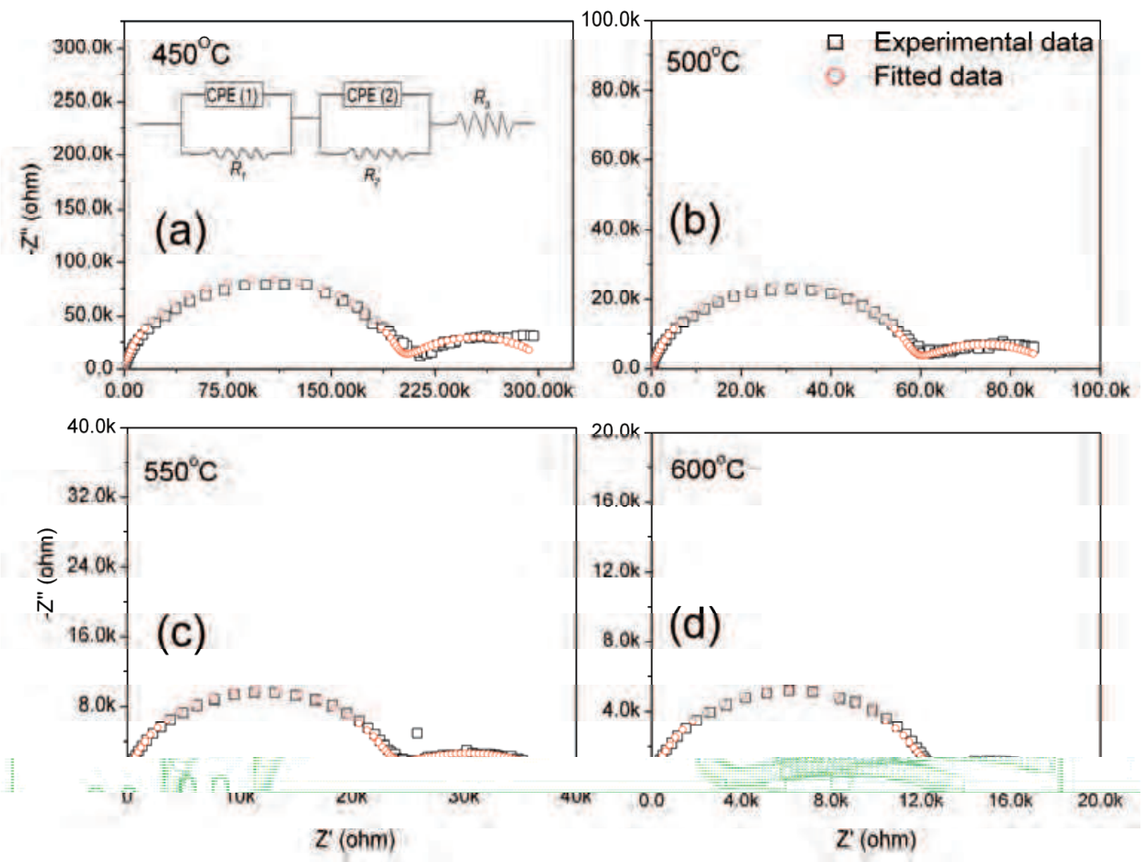

Fig. 7. Cole-Cole plots for x=0.025 BITWC samples at various temperatures.

experimental data. The capacitors in the equivalent circuit are universal capacitors ($C^* = A(i\omega)^{n-1}$), as introduced by Jonscher (Jonscher, 1977). Fitted parameters are reported in the Table II.

In order to study the relaxation mechanism for various compositions, the plots of (Z''/Z''_{max}) versus f/f_{max} are shown in Fig. 8 for the compositions under study at 600 °C. It is to be noted that relaxation peaks are completely overlapped. This indicates that the relaxation mechanism is invariant with W/Cr content. However, the plots have not merged in the lower frequency regime. It is due to the extrinsic phenomenon associated with the samples.

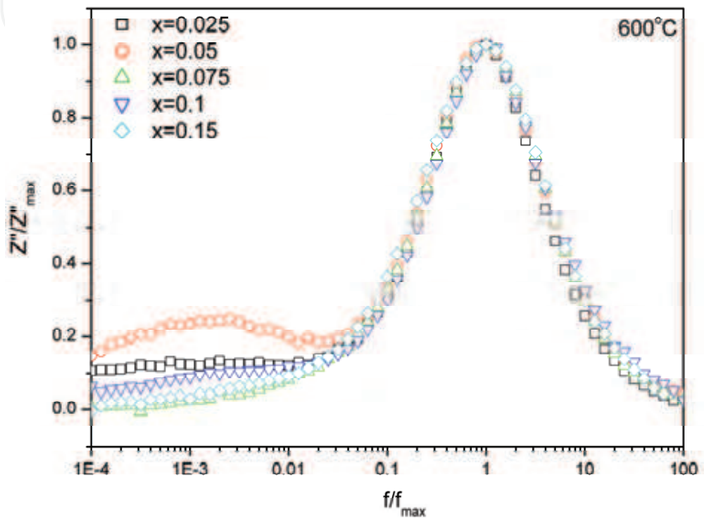

Fig. 8. Scaling plots for various values of x at a temperature of 600°C.

Dielectric constant and dielectric loss were calculated at various frequencies and temperatures (for the compositions under study) from the impedance data using the following relations:

$$\varepsilon' = \frac{-Z''}{\omega C_o \left(Z'^2 + Z''^2\right)} \tag{5}$$

$$\tan\delta = \frac{Z'}{-Z''} \tag{6}$$

where C_o is the equivalent vacuum capacitance $(= \varepsilon_o A / t)$ of the sample. A and t are area and thickness of the sample. Fig. 9 shows the dielectric permittivity and dielectric loss (tanδ) of W/Cr-doped BIT as a function of temperature measured at a frequency of 100 kHz. The dielectric peaks occur when the temperature is higher than 640 °C, which corresponds to the Curie temperatures. The Curie temperatures of BITWC are found to be slightly lower than that of BIT ceramic, and gradually decreased from 675 to 640 °C with increasing W/Cr content, which may partially arise from the difference of ionic radii (W^{6+}: 0.62 Å, Cr^{3+}: 0.52 Å, and Ti^{4+}: 0.605 Å) and partially result from an decrease in the lattice distortion (Kan, 2004; Lopatin, 1989; Nagata, 2004; Villegas, 2004). A small hump is observed in temperature dependence dielectric constant plots for higher compositions of BITWC ceramics (x > 0.075)

(as shown in inset of Fig. 9). This may be due to the presence of secondary phase in the ceramics (Hyatt, 2005; Luo, 2001). There is a sudden increase of loss (tan δ) in the curve, with a peak position slightly below the T_c. After the T_c, the loss (tan δ) reaches a minimum value and then begins to increase once again. This dielectric loss valley is corresponding to the dielectric peak, i.e., the Curie temperature. The selected room temperature properties of BITWC ceramics are characterized and listed in Table III. With increasing of W/Cr contents, the Curie temperature and the dielectric loss decreased whilst the dielectric permittivity and loss vary sluggishly.

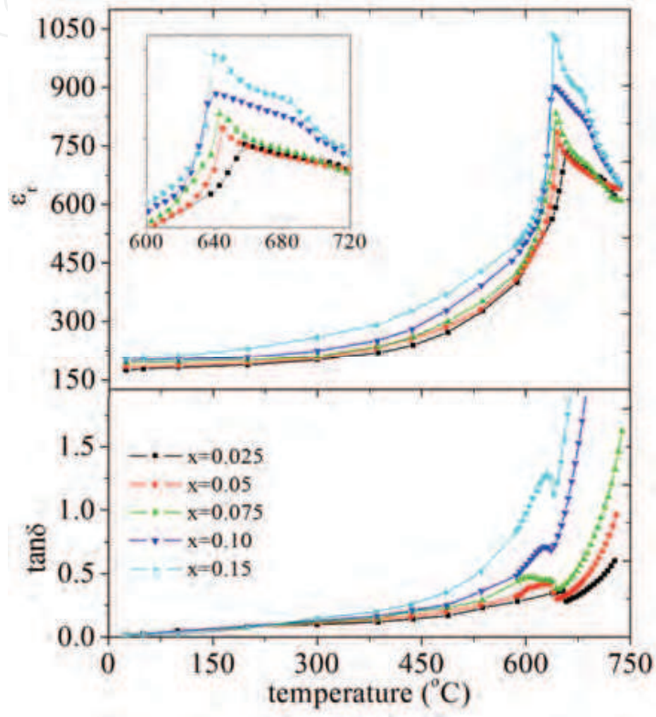

Fig. 9. Temperature dependence of dielectric constant and loss for the BITWC ceramics on W/Cr content.

In order to further elucidate the transport mechanism in the present ceramics, the electrical conductivity at different temperatures is studied. Electrical conductivity can be calculated from the dielectric data as:

$$\sigma(\omega) = \omega.\varepsilon_o.\varepsilon^{'}.\tan\delta \tag{7}$$

where ω is the angular frequency and ε_o is the vacuum permittivity. Fig. 10 shows the frequency dependent (0.1 Hz-3 MHz) electrical conductivity at various temperatures for 0.025BITWC. Similar trends were found for other samples which are not mentioned in here Fig. 10. The electrical conductivity depends on frequency according to the "universal dynamic response" and can be related as $\sigma(\omega) = \sigma_{DC} + A.\omega^n$, where A is the temperature dependent parameter and the exponent n is a characteristic parameter representing the many body interactions of the electrons, charges and impurities. It varies from 0 to 1 and for ideal Debye type behaviour it is equal to 1 (Jonscher, 1977). In Fig. 10, at all the

temperatures, the conductivity is independent of frequency at low frequency regime. Above a characteristic frequency, the conductivity increases with increase in frequency with characteristics ω^n dependence. The conductivity increases with increasing temperature due to thermal activation of conducting species in the samples. The frequency response of the other compositions also behaved similarly. Electrical conduction in BITWC ceramics is expected to result mainly from the defects presented in the lattice. These defects could come from the volatilisation of Bi_2O_3 during sintering, which could result in oxygen and bismuth vacancies. The variation of dc conductivity (σ_{DC}) with temperature can be described by Arrhenius equation as;

$$\sigma_{DC} = \sigma_o \exp\left(-E_{DC}/kT\right) \tag{8}$$

Where σ_o is pre-exponential factor and E_{DC} is activation energy associated with dc conductivity. Fig. 11 shows dc conductivity as a function of inverse of absolute temperature. From the slope of the linear fit, we can estimate activation energy associated with dc conduction. The variation of the activation energy with the W/Cr (x) content is depicted in the inset of Fig. 11. The activation energy (0.9 eV) for the conductivity of x=0.025 samples suggested an extrinsic conduction mechanism. With increasing W/Cr doping, the activation energy increased from ~0.9 to ~1.5 eV. This is associated with a change from extrinsic to intrinsic conductivity (Takahashi, 2003; Zhou, 2006; Zhang, 2009). It is well known that the intrinsic electronic conductivity activation energy is equal to half of the energy of the band gap (E_g). The reported value for the band gap is 3.3 eV for $Bi_4Ti_3O_{12}$ ceramics (Ehara, 1981) which is in close agreement with that of the present results (1.5 eV). It is interesting to note that the values for activation energy of dc conduction and electrical relaxation (Fig. 5) are in close agreement which indicates that the same ions are responsible for the both the processes (dc conduction and relaxation).

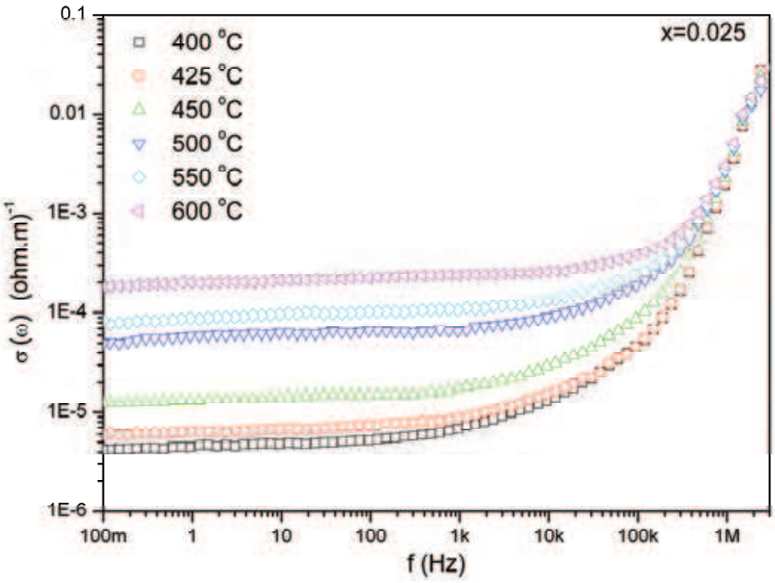

Fig. 10. Frequency dependent electrical conductivity at various temperatures.

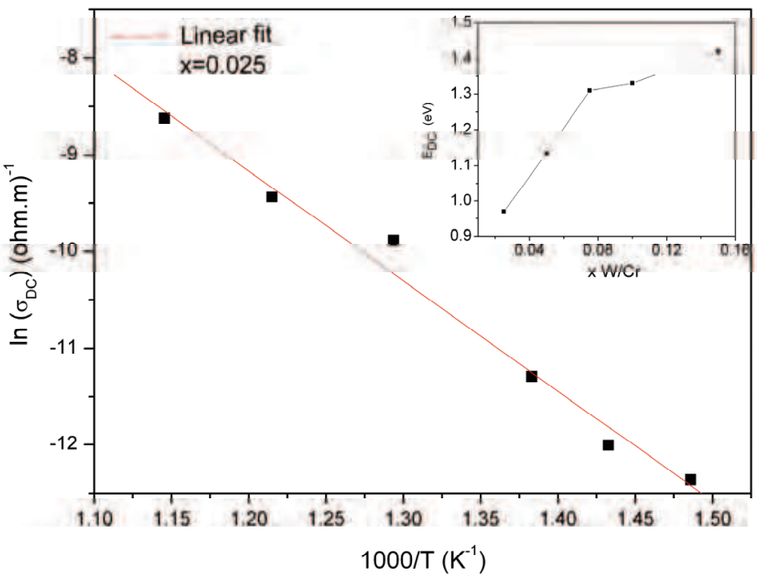

Fig. 11. Arrhenius plot for dc conductivity for x=0.025 sample and inset shows variation of activation energy with W/Cr content.

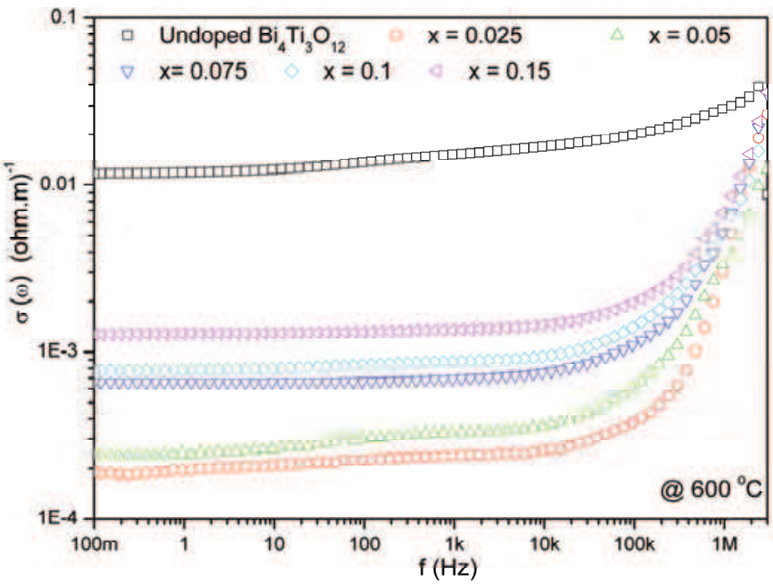

Fig. 12. Frequency dependent electrical conductivity for various W/Cr content

To further investigate the conductivity for all the compositions, we have plotted frequency dependent (0.1Hz-3MHz) electrical conductivity for all the compositions under study at 600 °C temperature as shown in Fig. 12. It is interesting to note that electrical conductivity of x=0.025 sample decreases significantly as compared with that of undoped BIT ceramics. Consequently conductivity increases with further increase in W/Cr content. In BIT ceramics, hole compensation of bismuth vacancies promotes p-type electronic conductivity. Under charge neutrality restriction, when W^{6+} substitutes Ti^{4+}, two positive charge centers at W site

and two electrons will be created. These electrons neutralize the influence of the holes. The conductivity decreases with donor doping to a minimum value where the concentration of electron holes matches the electron concentration (p=n). With a further increase in the donor (W^{+6}) concentration the conductivity becomes n-type and starts to increase again. The minimum conductivity appears at a lower W/Cr content doped BIT ceramics (x=0.025). Presence of secondary phase in higher concentration doped (x>0.075) ceramics can also play crucial role in the conductivity behaviour (Hyatt et al. 2005; Jardiel et al. 2006). It is reported that the $Bi_6Ti_3WO_{18}$ ceramics have higher conductivity than $Bi_4Ti_3O_{12}$ ceramics which results higher conductivity associated with the ceramics of higher concentration (x > 0.075). However, it is reported in the literature that the conductivity decreases up to concentration of x = 0.08 and consequently increases in sluggish manner with increase in the W doping (Jardiel, 2008). The reported value of dc conductivity at 600 °C is 3.2 × 10^{-5} (ohm·cm)$^{-1}$ for the W doping concentration of 0.05 (Jardiel, 2008). While in the present investigations, the value of dc conductivity is found to be 2.38 × 10^{-6} (ohm·cm)$^{-1}$ for the x=0.05 W/Cr doping at 600 °C. This difference in the value of electrical conductivity can be attributed to microscopic heterogeneity and random arrangement of cations in the structure due to the presence of Cr ions along with W and Ti ions at B-site. The interaction between the cations controls the conduction and dielectric mechanisms of the present ceramics. A defect chemistry expression for W doping can be written as

$$WO_3 + V_o^{\bullet\bullet} \xleftarrow{TiO_2} 0.5W_{Ti}^{\bullet\bullet} + 3O_{\circ} \tag{9}$$

It shows that the oxygen vacancies are reduced upon the substitution of donor W^{6+} ion for Ti^{4+}. Hence, it is reasonable to believe that the conductivity in BIT ceramics is suppressed by donor doping.

The piezoelectric constant (d_{33}) was measured at room temperature for all the compositions. All the samples were electrically poled prior to piezoelectric measurements. It is interesting to observe that the sample for x=0.025 has higher d_{33} coefficient than that of the other compositions (Table III). It is related to the fact that composition corresponding to x=0.025 has lowest conductivity among the samples studied in this work and thus allowing for better poling. The gained increment in d_{33} by W/Cr co-doping is very desirable, indicating a significant improved piezoelectric property due to W/Cr modification.

$Bi_4Ti_{3-x}W_xO_{12+x}$ +0.2wt%Cr_2O_3	T_c (°C)	ε', at 100 kHz,	tan δ at 100 kHz,	d_{33}(pC N^{-1})
x=0.025	658	178	0.02	22
x=0.050	650	186	0.021	17
x=0.075	648	197	0.023	16
x=0.100	645	205	0.028	14
x=0.150	640	211	0.028	12

Table 3. Physical characteristics for W/Cr modified BIT ceramics at room temperature.

The crystallographic evolution and phase analysis of $Bi_4Ti_3O_{12}$:W/Cr ceramics were determined by the XRD and the microstructural morphology was studied by SEM analysis.

The modification of W/Cr significantly improved the piezoelectric activity of the $Bi_4Ti_3O_{12}$:W/Cr ceramics. The Curie temperature decreased slightly with W/Cr modification increasing. Electrical relaxation mechanism was found to be similar for all the compositions. The excellent piezoelectric and dielectric properties coupled with high Curie temperature, demonstrated that the $Bi_4Ti_{2.975}W_{0.025}O_{12.025}$+0.2wt%$Cr_2O_3$ (x=0.025) ceramics are promising candidates for high temperature applications.

3. Nb/Ta modified $Bi_4Ti_3O_{12}$ ceramics

Doped BIT is of interest in high-temperature piezoelectric sensors, because it remains ferroelectric at T > 600 °C and offers relatively high piezoelectric property (Kumar, 2001; Nagata, 1999; Noguchi, Sugibuchi, 1975; Shimakawa, 2000; Subbarao, 1961; 2000; Shulman, 2000; Shimazu, 1980). High leakage current and domain pinning due to defects in undoped BIT have appeared as obstacles for further applications. Unfortunately, the piezoelectric effect in high Curie temperature BIT is relatively low, with coefficient values less than 10 pC N^{-1} for pure BIT and less than 20 pC N^{-1} for modified $Bi_4Ti_3O_{12}$. To improve the piezoelectric property, Nb/Ta co-modified BIT ceramics were fabricated by a conventional solid-state reaction process and the influence of the Nb_2O_5/Ta_2O_5 additive on the structure and electrical properties of the ceramics was investigated. The composition $Bi_4Ti_{3-2x}Nb_xTa_xO_{12}$ (BTNT, x=0, 0.01, 0.02, 0.04, 0.06) polycrystals were prepared by the conventional solid-state reaction technique.

To investigate the effect of Nb/Ta modified BIT ceramics on the phase stability, $Bi_4Ti_{3-2x}Nb_xTa_xO_{12}$ powders calcined at 800 °C for 4 h were prepared and their crystal structures were analyzed using XRD. Fig. 13 shows the XRD patterns of all samples. Diffraction data does not show any evidence of the formation of niobium and tantalum oxides or associated compounds that contain bismuth or titanium. This observation indicates that Nb/Ta ions in the BTNT ceramics do not form minority phase or segregate from the interior grain but dissolve into the perovskite lattice. Therefore, the BTNT ceramics maintains a layer structure similar to the perovskite BIT.

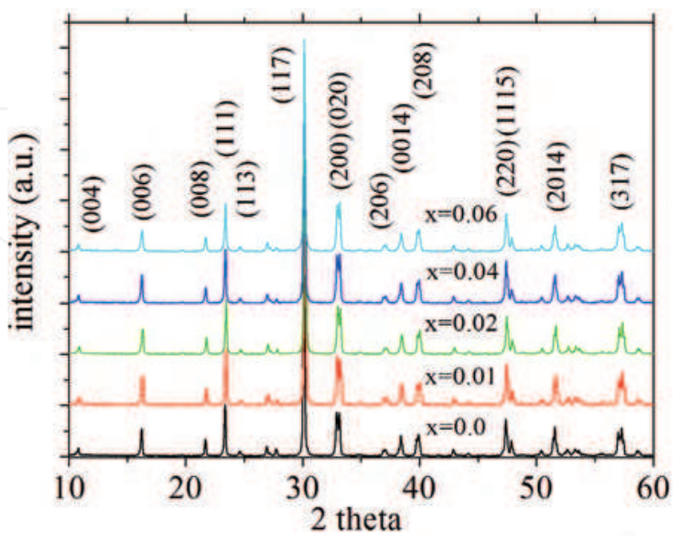

Fig. 13. XRD patterns of $Bi_4Ti_{3-2x}Nb_xTa_xO_{12}$ powders calcined at 800 °C for 4 h on different Nb/Ta amounts.

The microstructures of BTNT ceramics are shown in Fig. 14. As figure 14 show average grain size ranging from approximately 40 μm to 1μm in length decreased with increase of Nb/Ta amount, which suggested that the additive controlled the growth of the plate-like grains. The porosity was mainly located on grain boundaries. As is well known, both sintering and grain growth are closely associated with ion migration. Thus if the incorporation of Nb^{5+}/Ta^{5+} into BIT led to an increase in the activating energy for ion migration, a reduction in the rate of grain growth would be expected with increasing amounts of Nb/Ta. Furthermore, according to the sintering theory, the particle surface energy and grain boundary energy are the major driving forces for sintering and grain growth.

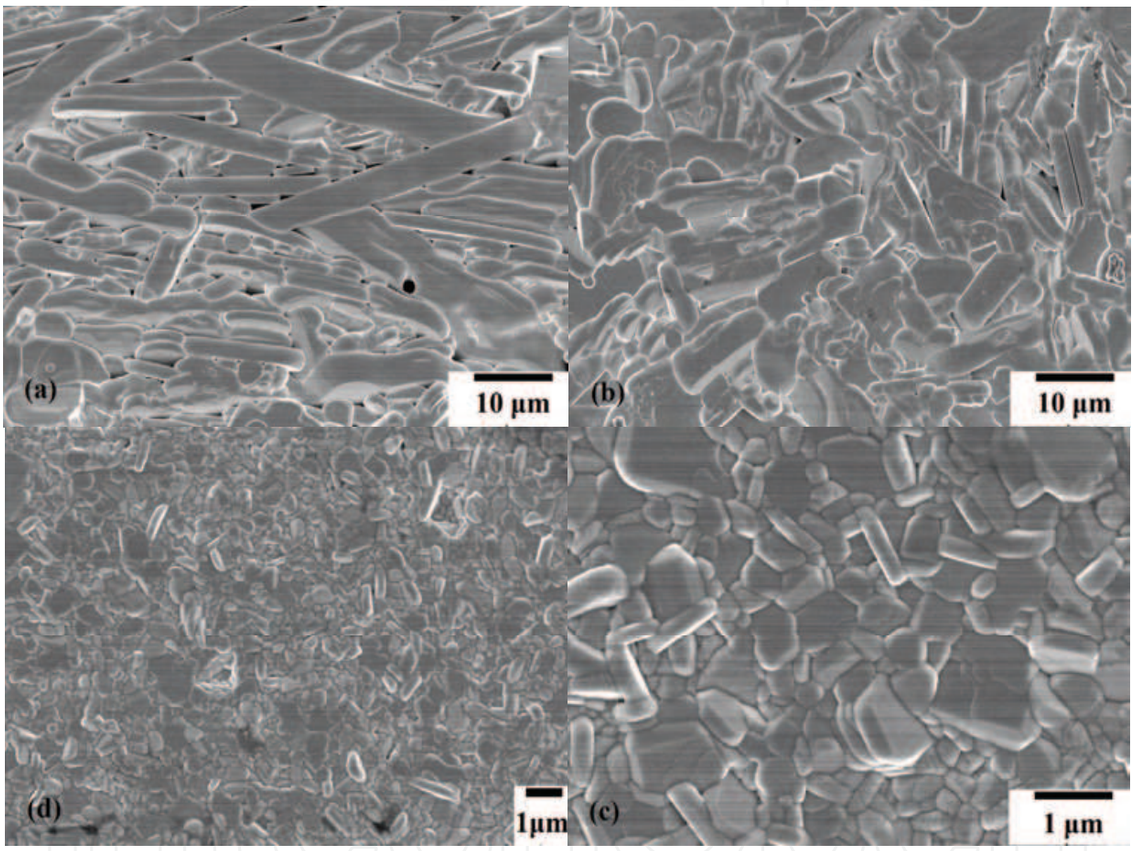

Fig. 14. SEM images of $Bi_4Ti_{3-2x}Nb_xTa_xO_{12}$ ceramics on different Nb/Ta amount: (a) x=0.01, (b) x=0.02, (c) x=0.04, (d) x=0.06.

BTNT ceramics sintered at the temperatures giving maximum density values were used for the measurement of dielectric property. Fig. 15 shows the permittivity, ε_r, and dielectric loss, tanδ, of Nb/Ta-doped BIT ceramics as a function of temperature measured at a frequency of 100 KHz. The Curie temperatures of BTNT ceramics are found to be slightly lower than that of BIT ceramic, and gradually decreased from 675 to 630 °C with increasing Nb/Ta amounts due to the contribution of space charge and ionic motion (Fouskova, 1970). Moreover, the phase transition peaks become broad and diffusive, which may result from the cation-exchange between Ti^{4+} in TiO_6 octahedra and Nb^{5+}/Ta^{5+} at the B sites to release the misfit strain due to the similar ionic radii (Nb: 0.69 Å, Ta: 0.64 Å, Ti: 0.605 Å). For the dielectric

loss, there is a sudden increase in the curve, with a peak position slightly below the Curie temperature, T_c. After the T_c, the dielectric loss reaches a minimum value and then begins to increase once again. With increasing Nb/Ta amounts the peaks of the dielectric loss shifted to the lower temperature and even became flatter. So the activation energy of oxygen vacancy correspondingly increased with the distortion of lattice after doping enhances its hopping barrier. It is clear that the introduction of the Nb^{5+}/Ta^{5+} at B-site in BIT as donor impurities can effectively reduce the oxygen vacancies, which may be elucidated by the defect reaction:

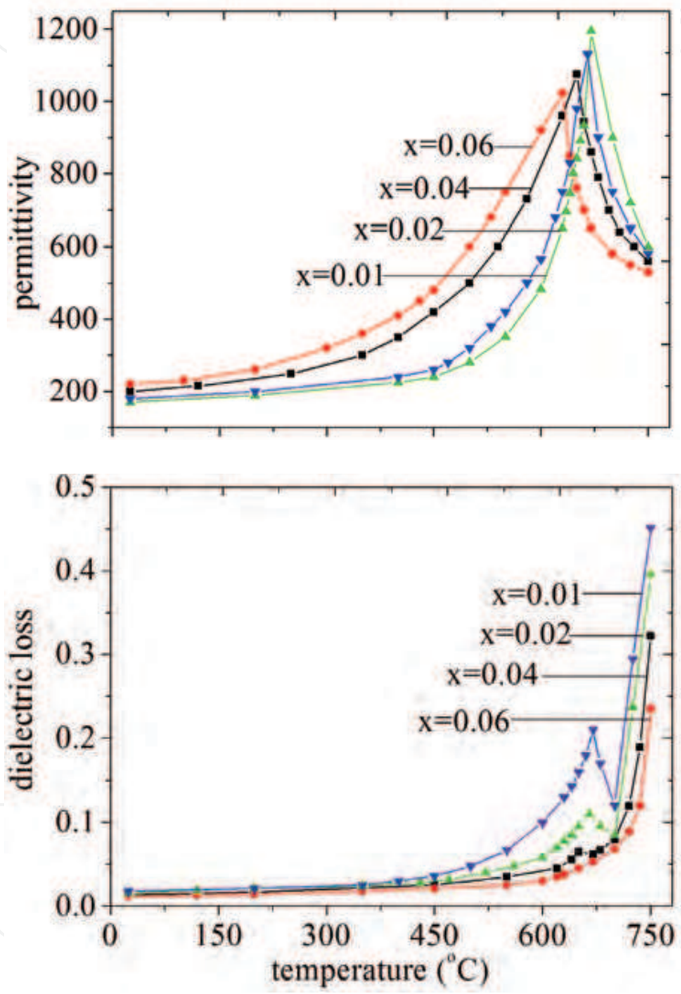

Fig. 15. Temperature dependence of permittivity and dielectric loss for BTNT ceramics on Nb/Ta amounts.

$$Nb_2O_5 + V_O^{\cdot\cdot} \rightarrow 2Nb_{Ti}^{\cdot} + 5O_o \quad \text{and} \quad Ta_2O_5 + V_O^{\cdot\cdot} \rightarrow 2Ta_{Ti}^{\cdot} + 5O_o \,. \tag{10}$$

A decrease of the oxygen vacancy after the Nb^{5+}/Ta^{5+} doping results in the depression of the dielectric loss peak, which was consistent with previous reports (Shulman, 2000, 1996; Villegas, 1999). Thus B-site doping of equal valence can screen the effect of oxygen vacancy, which is contributing to an enhancement of the dielectric property of BTNT ceramics.

The selected room temperature properties of BTNT ceramics as a function of Nb/Ta amounts are characterized. Fig. 16c shows the permittivity and dielectric loss of the BTNT ceramics as a function of Nb/Ta amount. It was found that the room temperature permittivity of BTNT ceramics increased drastically whilst the dielectric loss decreased due to the depression of the oxygen vacancies with increasing Nb/Ta amounts. Figure 16a and 16b show the piezoelectric coefficient d_{33} and Curie temperature T_c of the BTNT ceramics for varying amounts of Nb/Ta . The d_{33} values first increased and reached a maximum value of 26 pC N^{-1} for samples with x=0.01. However, previous research has shown that doping a small amount of Nb_2O_5 or Ta_2O_5 resulted in an increase in the d_{33}, from 8 to 20 pC N^{-1} (Shulman, 1996, Shulman, 2000). The gained increment in d_{33} by Nb/Ta co-doping is very desirable, indicating a significant improvement in the piezoelectric property. The change in piezoelectric properties was explained with a grain size effect, namely, a sound grain growth with the addition of Nb_2O_5/Ta_2O_5, enables a consummate development of ferroelectric domains and thus improves the piezoelectric properties. As a result, there may be more crystallographic directions suitable for polarization, facilitating piezoelectricity. Based on decreasing dielectric loss, it's proposed that the grain size effects play a dominant role in the piezoelectric response. On the other hand, with decrease in oxygen vacancies diffusing to the domain wall in bulk, the pinning of the domain wall can decrease and the number of available switching domain walls can increase, resulting in enhancement of the d_{33}. But a further increase of concentration of Nb/Ta in BIT could act as pinning centres for domain walls and reduce their contribution to the piezoelectric effect, which is consistent with the previous reports that the addition of Nb and other cations in perovskite layer with dimensional mismatch between perovskite and bismuth oxide layers (Armstrong, 1972). It also can be seen the Nb/Ta doping causes more drastic decrease in the values of T_c. Thermal annealing behavior for the control and Nb/Ta modified BIT ceramics are shown in Figure 16d, where the piezoelectric coefficient, d_{33} are plotted against the annealing temperature. The values of d_{33} of the BTNT ceramics show no obvious drop, when the annealing temperature is lower than 500 °C. This reveals that BTNT orthorhombic structured materials are very stable to thermal annealing. When annealing temperature is higher than 500 °C, about 74 % of T_c, the piezoelectric coefficient of all BTNT ceramics decreases sharply, and tends to zero when the annealing temperature is above T_c.

The *B*-site vacancies $Bi_4Ti_{3-2x}Nb_xTa_xO_{12}$ ceramics were synthesized by the solid-state reaction process. The analysis of the structure and the morphology were performed by XRD and FESEM. All the specimens maintained the orthorhombic structure and the addition of Nb_2O_5/Ta_2O_5 caused a remarkably suppressed grain growth, which plays the dominant role in the piezoelectric response. This work also presented the considerable influence of Nb_2O_5/Ta_2O_5 additive on the dielectric and piezoelectric properties. The Curie temperature, T_c, decreased from 675 to 630 °C while the permittivity increased drastically. The Nb/Ta doping at B-site could induce the distortion of oxygen octahedral and reduce the oxygen vacancy concentration by the compensating effect which is contributed to the enhancement of piezoelectric activity. The high piezoelectric coefficient d_{33} of $Bi_4Ti_{2.98}Nb_{0.01}Ta_{0.01}O_{12}$ ceramics controlled by precisely optimizing Nb/Ta amounts is found to be 26 pC N^{-1}. All measurements demonstrated that BTNT ceramics are the promising candidates for high temperature applications.

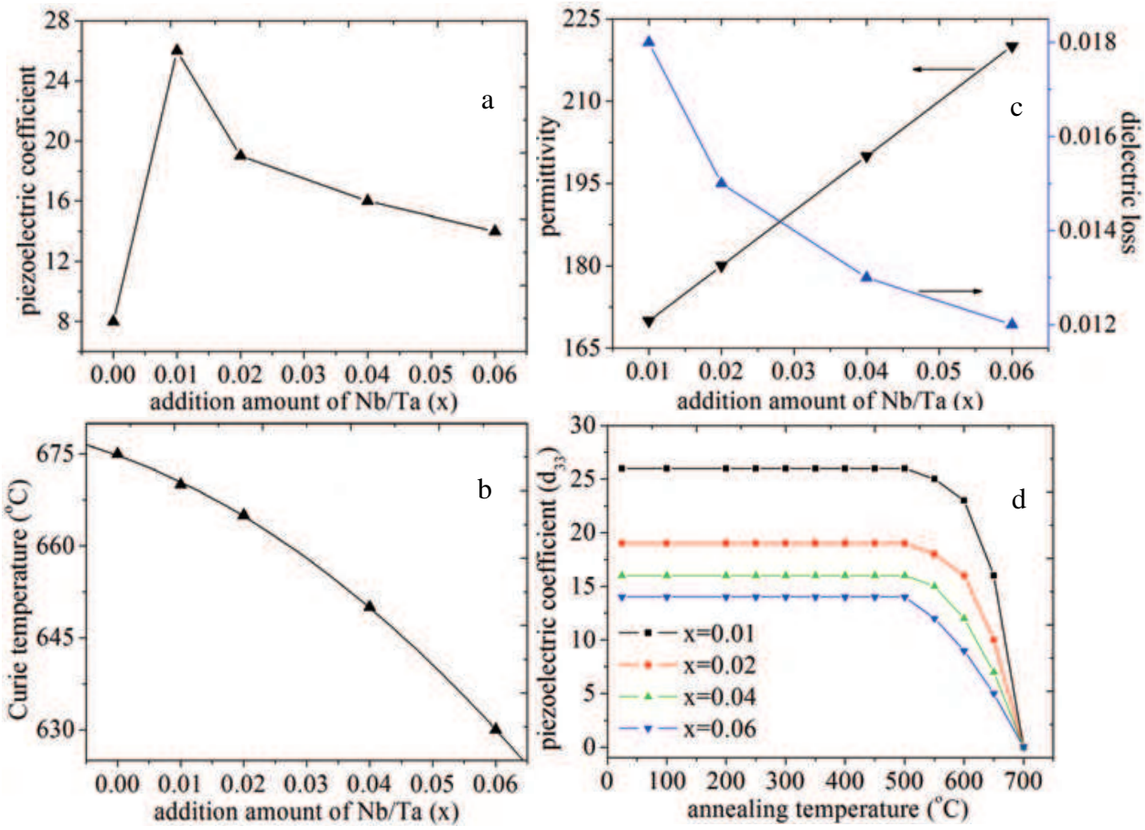

Fig. 16. Properties of $Bi_4Ti_{3-2x}Nb_xTa_xO_{12}$ ceramics for different Nb/Ta amounts at room temperature (a,b,c), effect of annealing temperature for 2 h on d_{33} of $Bi_4Ti_{3-2x}Nb_xTa_xO_{12}$ ceramics (d).

4. Nb/Ta/Sb modified $Bi_4Ti_3O_{12}$ ceramics

Lead-based piezoelectric ceramics such as $Pb(Zr,Ti)O_3$ (PZT), are widely used in piezoelectric actuators, sensors, and transducers due to their high relative permittivity, large remnant polarization, and excellent piezoelectric coefficients (Jaffe, 1971; Uchino, 2000). However, evaporation of toxic lead oxides during high temperature sintering produces environmental toxic burden and also generates instability of the composition and electrical properties of the ceramics. Thus, investigation of the possible use of ecologically clean lead-free ceramics in the field of science and technology is of great interest.

Bismuth titanate, $Bi_4Ti_3O_{12}$ (BIT) is considered to be an excellent candidate as a key lead-free piezoelectric material owing to promising piezoelectric and ferroelectric properties. It is also a promising material for high temperature piezoelectric applications because of the high Curie temperature. However, as the spontaneous polarization movements are restricted to the *a*(*b*) plane of the unit cell (the *c*-axis component can be neglected), the ferroelectric and piezoelectric properties are much lower than those of PZT materials. It is likely, the piezoelectricity of pure BIT ceramics is low (d_{33} < 8 pC N^{-1}), due to the fact that it has high electrical conductivity and high coercive field which impedes the poling process (Ahn, 2009; Hou, 2010; Shulman, 2000, 1996; Villegas, 2004). The piezoelectric properties can be enhanced by grain orientation techniques (Jones, 2005; Zhang, 2005). However, these

processing methods such as hot forging or tape casting methods are not as cost effective as the production of ceramics via traditional powder pressing technologies. So, it is favourable to optimize piezoelectric properties via structural modification using appropriate doping. In this context, cations substitution to improve the piezoelectric properties of BIT have been considered and explored. It has been shown that the doping with donor cations such as Nb^{5+}, W^{6+} or Ta^{5+} in the Ti^{4+} positions decreases electrical conductivity and improves piezoelectric properties of BIT ceramics (Azurmendi, 2006; Hou et al, 2010; Hong, 2000). We have reported that the value of d_{33} was 26 pC N^{-1} for Nb/Ta doped BIT ceramics, fabricated via the conventional solid state reaction route (Hou, 2009).

It is noted that the studies concerning the effect of Sb doped lead-free piezoelectric ceramics have been reported earlier, exhibiting high-performance piezoelectric and dielectric properties (Saito, 2004; Zhao, 2008; Zhang, 2010). However, reports on Sb-doped BIT ceramics are scarce. To further study the piezoelectric property, Sb_2O_3 has been considered for modifying $Bi_4Ti_{3-2x}Nb_xTa_xO_{12}$ (BTNT) ceramics via the conventional solid-state reaction route. The influence of the Sb_2O_3 additive on the structural, morphological, dielectric, electrical conductivity and piezoelectric properties of the ceramics is investigated in this work.

Fig. 17 shows XRD patterns of BTNTS powders calcined at 800 °C for 4 h. The XRD analysis of BTNTS ceramic powders revealed the presence of BTNTS phase. Therefore, the BTNTS ceramics in the Sb substituted structure can maintain a layer perovskite structure similar to the parent BIT perovskite.

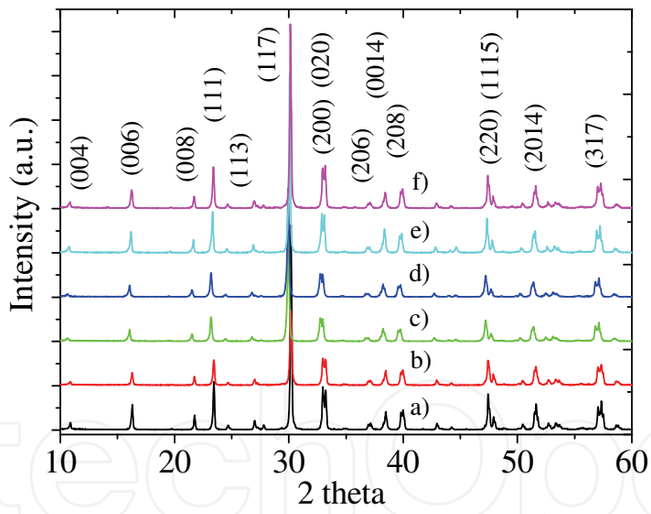

Fig. 17. XRD patterns of BTNTS powders calcined at 800 °C for 4 h with varying concentration of Sb_2O_3: a) 0BTNTS, b) 2BTNTS, c) 4BTNTS, d) 6BTNTS, e) 8BTNTS, f) 10BTNTS

The microstructures of BTNTS ceramics are shown in Fig. 18. The average grain size can be observed to be varying with the content of Sb_2O_3, suggesting that the additive controlled the growth of the plate-like grains of BTNTS. 8BTNTS ceramic has slight larger grains while there is a small variation in grain size for the other samples. Change in the microstructure with doping content is due to the reported formation of liquid phase (sillenite phase) which is generally observed during the synthesis of BIT (Rojero et al. 2010) (Although, this secondary phase was not detected in XRD due to small amounts (Fig. 17)). This liquid phase is increasing

with the increase in Sb_2O_3 content and avail grain growth. 8BTNTS ceramic has larger grain size due to the presence of larger quantity of sillenite phase. However 10BTNTS ceramic samples were observed with smaller grains (Fig. 18(f)). It may be due to excess amount of antimony (after formation of solid solution) which reacted with sillenite phase and reduced it.

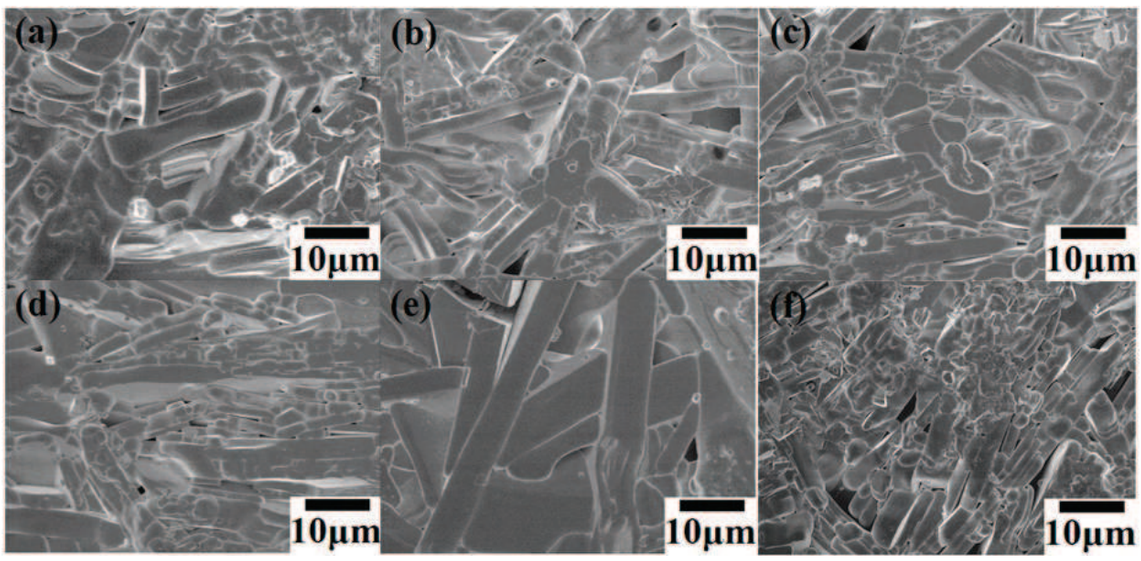

Fig. 18. SEM images of BTNTS ceramics with different Sb_2O_3 content: a) 0BTNTS, b) 2BTNTS, c) 4BTNTS, d) 6BTNTS, e) 8BTNTS, f) 10BTNTS

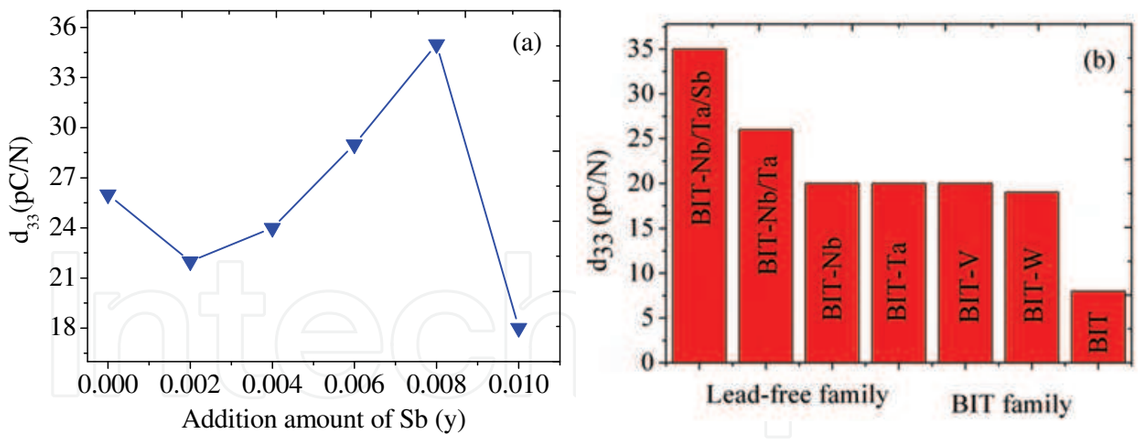

Fig. 19. Piezoelectric coefficients (d_{33}) of BTNTS ceramics with different Sb_2O_3 content at room temperature (a), comparison of d_{33} among 8BTNTS and BIT family (b) (BIT, BIT-W, BIT-Ta BIT-Nb, BIT-V, BIT-Nb/Ta)

Fig. 19 shows the variation of the piezoelectric coefficient (d_{33}) with respect to the content of Sb_2O_3 for the BTNTS ceramics. The value of d_{33} was found to be highest (35 pC N^{-1}) for 8BTNTS ceramics. The d_{33} value is lower with deviation from 8BTNTS composition in both directions of increasing or decreasing the content of Sb_2O_3, but in all other compositions from 0 to 8, exceeds the hitherto maximum value of ~20 pC N^{-1}. The d_{33} (35 pC N^{-1}) of

8BTNTS is 337.5%, 84.2%, 75% and 34.6% higher than that of BIT (Shulman, 1996), W-doped BIT (Zhang, 2004), V-doped BIT (Tang, 2006), Nb-doped BIT (Shulman, 2000), Ta-doped BIT (Hong, 2000), and Nb/Ta-doped BIT (Hou et al, 2009). The thermal annealing behaviors for the 0BTNTS, 8BTNTS and 10BTNTS ceramics are shown in Fig. 20, where the piezoelectric coefficient, d_{33} are dependent on the annealing temperature. The d_{33} values of the BTNTS ceramics show no obvious drop, when the annealing temperature is lower than 500 °C. This indicates that BTNTS monoclinic structured materials are very stable to thermal annealing. When annealing temperature is higher than 500 °C, the piezoelectric coefficients of the 0BTNTS, 8BTNTS and 10BTNTS ceramics decrease sharply, and tend to zero when the annealing temperature is above Curie temperature (675 °C). No obvious degradation of the 0BTNTS, 8BTNTS and 10BTNTS ceramics is observed below 500 °C.

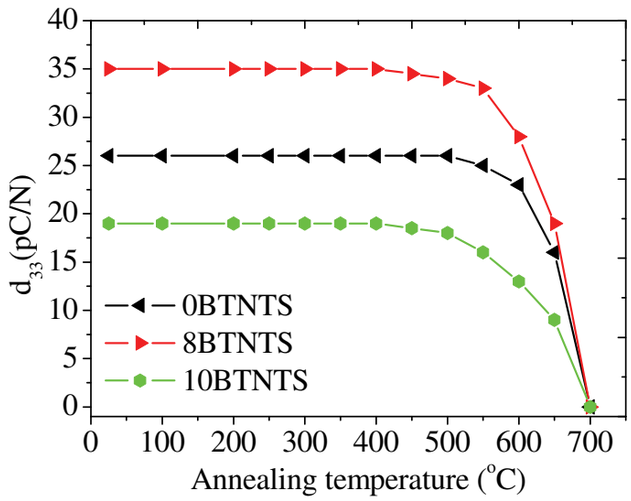

Fig. 20. Effect of annealing temperature for 2 h on d_{33} for 0BTNTS, 8BTNTS and 10BTNTS ceramics

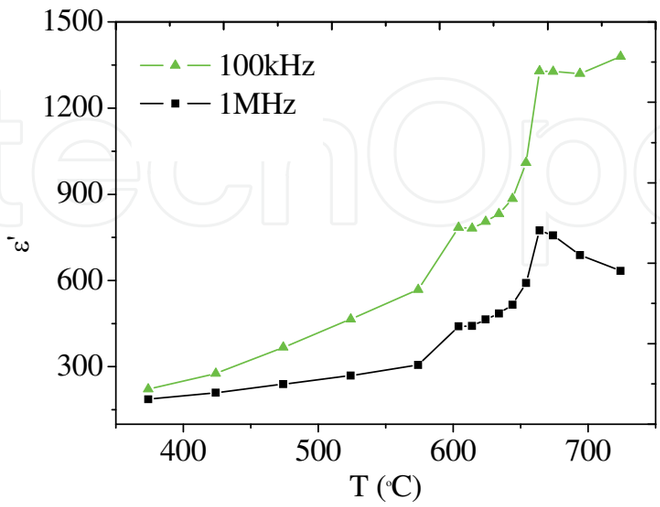

Fig. 21. Temperature dependence of permittivity for $Bi_4Ti_{2.98}Nb_{0.01}Ta_{0.002}Sb_{0.008}O_{12}$ ceramics at 100 kHz and 1 MHz

It is well known that the electrical properties are of fundamental importance for the piezoelectric applications. It is therefore worthwhile to investigate these properties over a moderately wide frequency and temperature range for 8BTNTS samples (highest d_{33} value among the $Bi_4Ti_3O_{12}$–based ceramics). Fig. 21 shows the permittivity, ε_r, of $Bi_4Ti_{2.98}Nb_{0.01}Ta_{0.002}Sb_{0.008}O_{12}$ ceramics as a function of the temperature measured at 100 KHz and 1 MHz. Two peaks are observed at around 600 °C and 660 °C (at both frequencies (100 KHz and 1 MHz)) corresponding to the phase transformation of secondary and 8BTNTS phases, respectively. To confirm our results, the differential scanning calorimetric trace for 8BTNTS ceramics is depicted in Fig. 22. The sharp peak at 664 °C is associated with the phase transformation and ascribed as a Curie temperature which is in close agreement with that of the permittivity versus the temperature plots (Fig. 21).Though, another peak (600°C) was not detected in DSC trace.

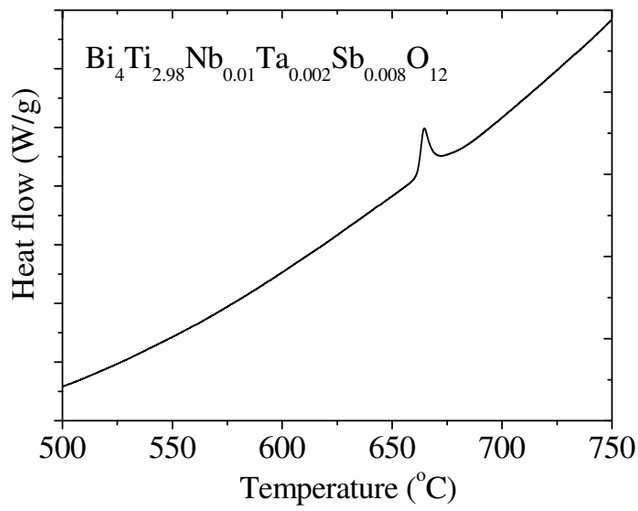

Fig. 22. DSC curve of $Bi_4Ti_{2.98}Nb_{0.01}Ta_{0.002}Sb_{0.008}O_{12}$ ceramic

Fig. 23 depicts the frequency dependent (0.1 Hz~3 MHz) electrical conductivity for all the compositions at 600 °C. It is interesting to note that the electrical conductivity of 8BTNTS decreases significantly as compared with that of other ceramics. This difference in the value of electrical conductivity may be attributed to microscopic heterogeneity and random arrangement of cations in the structure due to Sb/Nb/Ta/Ti ions at B-site. We have reported that addition of Nb and Ta can directly introduce additional electrons for neutralizing the effect of *p*-type conductivity commonly observed in pure BIT (Shulman, 1996). These dopants also decrease the concentration of oxygen vacancy in the BIT doped by Nb/Ta. Sb has 3+ oxidation state in Sb_2O_3 (0.76 Å ionic radii) and can not be fitted on Ti^{4+} site (0.605 Å). However it is reported (Peiteado, 2006) that Sb^{3+} is unstable above 500 °C and completely transform into Sb^{5+} (0.60 Å ionic radii) in the presence of Bi_2O_3 oxide. It indicates that in the present study, Sb^{5+} ions are accommodated at Ti^{4+} sites since samples were sintered at 1100 °C. The amount of Sb added to the Nb/Ta doped BIT is in relatively small concentrations at the B-sites in the perovskite structure. In addition to the effect of reducing *p*-type conductivity, and decreasing oxygen vacancy concentration we can expect greater domain wall movement. Thus, Sb has the effect of controlling this switch to *n*-type conductivity while not impairing the decrease in *p*-type conductivity. In addition to donor

effect of antimony, it is noticed that the microstructures of these samples are also doping dependent (Fig. 18). Scanning electron micrographs (Fig. 18) show that 8BTNTS ceramics have larger grain size than that of the other investigated samples. It is reported that microstructure plays for electrical properties of BIT ceramics (Jardiel, 2006). Due to the decrease in electrical conductivity, the polarization is aided, facilitating the improved piezoelectricity. The possible explanation may be ascribed to decrease in the concentration of oxygen vacancies that can diffuse to domain walls in the piezoelectric ceramic, resulting in lowering the pinning of the domain walls, thus increasing the number of available switching domain walls and resulting in the enhancement of d_{33} (Zhang, 2006).

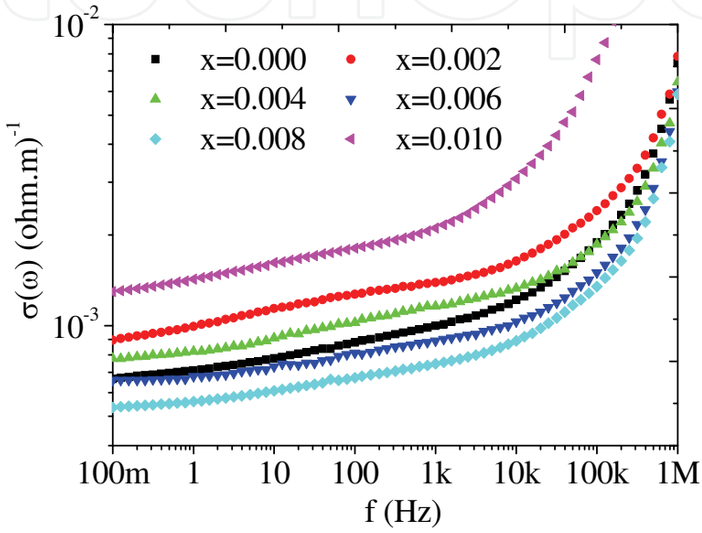

Fig. 23. Electrical conductivity of BTNTS ceramics with different Sb_2O_3 content at 600 °C

In order to understand the conductivity mechanism in BTNTS ceramics, the ac conductivity plots that were obtained in the 300~600 °C temperature range for the 8BTNTS ceramics are shown in Fig. 24. The conductivity increases with increasing temperature due to thermal activation of conducting species in the samples. It exhibits two relaxations at different frequency region. The low frequency relaxation can be attributed to the grain boundary. As the frequency increases, the grain boundary resistance might become less than that of grain and grains dominate conductivity. The resistance and capacitance associated with grain and grain boundary interplay between their capacitive and dielectric contributions depending upon the frequency range. The high frequency conductivity is entirely due to the hopping of localized charge carriers. The bulk DC conductivity is difficult to ascertain from the above data (Fig. 24) because of significant contributions of grain boundary to the conductivity in low frequency regime.

The electric modulus approach was invoked to elucidate the electrical transport mechanism in 8BTNTS ceramics. The physical nature of the electric modulus (Macedo, 1972) is used to make a correlation between the conductivity and the relaxation of ions in these materials. This approach can effectively be employed to study bulk electrical behaviour of the moderately conducting samples. The complex electric modulus (M^*) is defined in terms of the complex dielectric constant (ε^*) and is represented as:

$$M^* = (\varepsilon^*)^{-1} \tag{11}$$

$$M' + iM'' = \frac{\varepsilon_r'}{(\varepsilon_r')^2 + (\varepsilon_r'')^2} + i\frac{\varepsilon_r''}{(\varepsilon_r')^2 + (\varepsilon_r'')^2} \tag{12}$$

where M', M'' and ε_r', ε_r'' are the real and imaginary parts of the electric modulus and dielectric constant, respectively. Effects of electrode polarization and the electrical conductivity can be suppressed using the electric modulus formalism. The real and imaginary parts of the modulus at different temperatures are calculated using Eq. 12 for the 8BTNTS ceramics and depicted in Figs. 25 (a) and 25 (b), respectively.

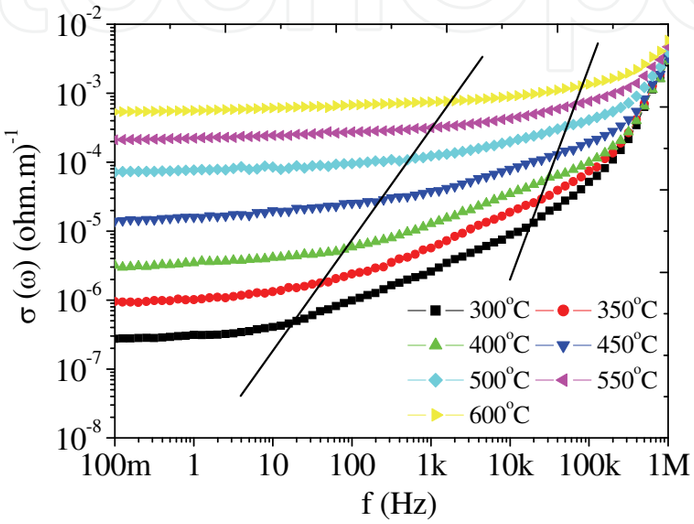

Fig. 24. Frequency dependence of ac conductivity at different temperatures for 8BTNTS ceramics

It is seen from Fig. 25 (a) that at low frequencies, M' approaches zero at all the temperatures under study suggesting the suppression of electrode polarization effects. M' reaches a maximum value corresponding to $M_\infty = (\varepsilon_\infty)^{-1}$ due to the relaxation process. It is also observed that the value of M_∞ decreases with the increase in temperature. The imaginary part of the electric modulus (Fig. 25 (b)) is indicative of the energy loss under electric field. The M'' peak shifts to higher frequencies with increasing temperature. This suggests the involvement of temperature-dependent relaxation processes in the present ceramics. The frequency region below the M'' peak indicates the range in which ions drift to long distances. In the frequency range which is above the peak, the ions are spatially confined to potential wells and free to move only within the wells. The frequency range where the peak occurs is suggestive of the transition from long-range to short-range mobility of ions.

The relaxation time associated with the process was determined from the plot of M'' versus frequency. The activation energy involved in the relaxation process of ions can be obtained from the temperature dependent relaxation frequency (f_{max}) as:

$$f_{max} = f_o \exp\left(-\frac{E_R}{kT}\right) \tag{13}$$

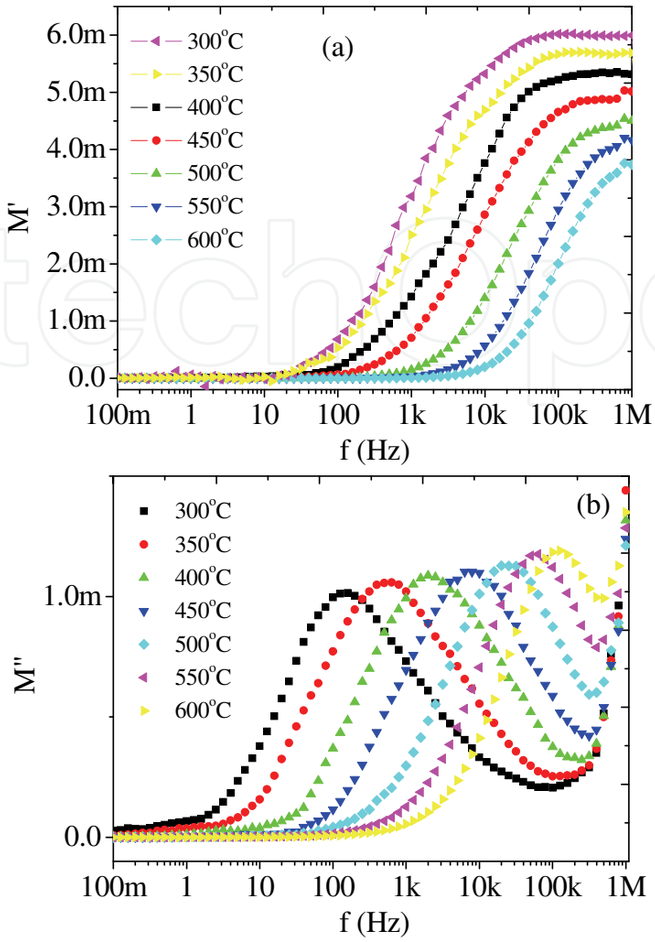

Fig. 25. (a) Real and (b) imaginary parts of the electric modulus as a function of frequency at different temperatures for 8BTNTS ceramics

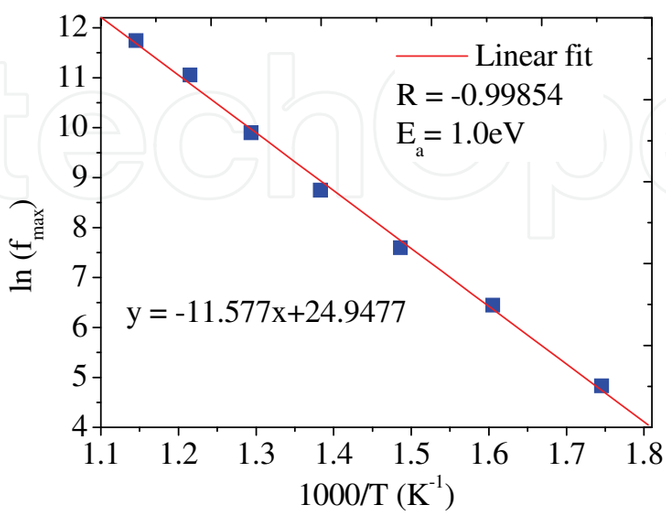

Fig. 26. ln (f_{max}) versus 1000/T for 8BTNTS ceramics

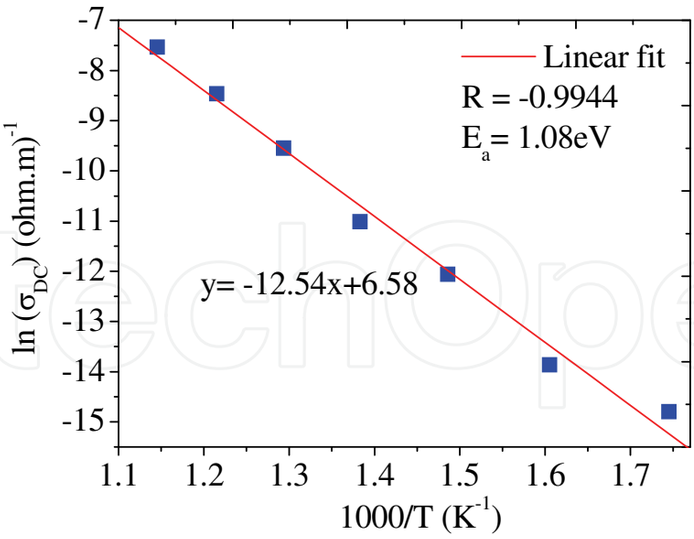

Fig. 27. ln (σ_{DC}) versus 1000/T for 8BTNTS ceramics

where E_R is the activation energy associated with the relaxation process, f_o is the pre-exponential factor, k is the Boltzmann constant and T is the absolute temperature. Fig. 26 shows a plot between ln(f_{max}) and 1000/T along with the theoretical fit (solid line) to the above equation (Eq. 13). The value that is obtained for E_R is 1.00 ± 0.03 eV, which is ascribed to the motion of oxygen ions and is consistent with more reported in the literature. The value of activation energy for 8BTNTS ceramics is higher than that of activation energy reported for pure BIT (Uchino, 2000). An increase in the activation energy as compared to BIT is an indication of the reduction of oxygen vacancies in 8BTNTS ceramics. This is due to the fact that the hole compensation of bismuth vacancies promotes p-type electronic conductivity. When Sb^{5+}&Nb^{5+}&Ta^{5+} ions substitute Ti^{4+} and electrons will be created under charge neutrality restriction. These electrons neutralize the influence of the holes. The conductivity decreases with donor doping to a minimum value where the concentration of electron holes matches the electron concentration (p = n). With a further increase in the donor (Sb^{5+}&Nb^{5+}&Ta^{5+}) concentration the conductivity becomes n-type and starts to increase again.

The electric modulus can be expressed as the Fourier transform of a relaxation function ϕ(t):

$$M^* = M_\infty \left[1 - \int_0^\infty \exp(-\omega t) \left(-\frac{d\varphi}{dt} \right) dt \right] \tag{14}$$

where the function ϕ(t) is the time evolution of the electric field within the materials and is usually taken as the Kohlrausch-Williams-Watts (KWW) function (Kohlrausch, 1954; Williams, 1970):

$$\varphi(t) = \exp\left[-\left(t / \tau_m \right)^\beta \right] \tag{15}$$

where τ_m is the conductivity relaxation time and the exponent β ($0 < \beta < 1$) indicates the deviation from Debye type relaxation. The smaller the value of β, the larger is the deviation

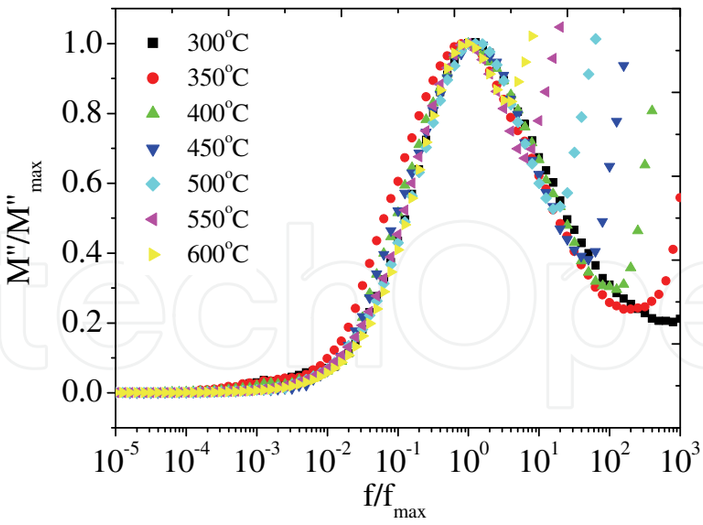

Fig. 28. Normalized plots of electric modulus against normalized frequency at various temperatures for 8BTNTS ceramics

from Debye-type relaxation. When β is close to zero, there exists a strong correlation between the hopping ions and its neighbouring ions. The β was calculated at different temperatures using the electric modulus formalism. For the ideal Debye type relaxation, the full-width half maximum (FWHM) of imaginary part of electric modulus is 1.14 decades. Therefore, β can be defined as 1.14/FWHM. One can estimate DC conductivity at different temperatures using the electrical relaxation data. The DC conductivity can be expressed as (Ngai, 1984):

$$\sigma_{DC}(T) = \frac{\varepsilon_o}{M_\infty(T) * \tau_m(T)} \left[\frac{\beta}{\Gamma\left(1/\beta\right)} \right] \tag{16}$$

where ε_o is the free space dielectric constant, $M_\infty(T)$ is the reciprocal of high frequency dielectric constant and $\tau_m(T)(1/2\pi f_{max})$ is the temperature dependent relaxation time. This equation is applicable to a variety of materials with low concentrations of charge carriers (Takahashi, 2004; Vaish, 2009). Calculation for DC conductivity from AC conductivity formalism causes a large error (due to electrode effect) that can be circumvented from the electrical relaxation formalism. Fig. 27 shows the DC conductivity data obtained from the above expression (Eq. 16) at various temperatures. The activation energy for the DC conductivity was calculated from the plot of $\ln(\sigma_{DC})$ versus $1000/T$ for BTNTS ceramics, which is shown in Fig. 27. The plot is found to be linear and fitted using following the Arrhenius equation,

$$\sigma_{DC}(T) = B \exp\left(-E_{DC}/kT\right) \tag{17}$$

where B is the pre-exponential factor and E_{DC} is the activation energy for the DC conduction. The activation energy is calculated from the slope of the fitted line and found to be 1.08 ± 0.02 eV. This value for activation energy is in close agreement with the activation energy for

electrical relaxation. Fig. 28 represents the normalized plots of electric modulus M'' as a function of frequency wherein the frequency is scaled by the peak frequency. A perfect overlapping of all the curves on a single master curve is not found. This shows that the conduction mechanism changed with temperature which is in good agreement with that of reported in literature (Takahashi et al 2004). Takahashi et al. reported that BIT exhibits mixed (ionic-p-type) conduction at high temperature and ionic conductivity was larger than hole conductivity in Curie temperature range.

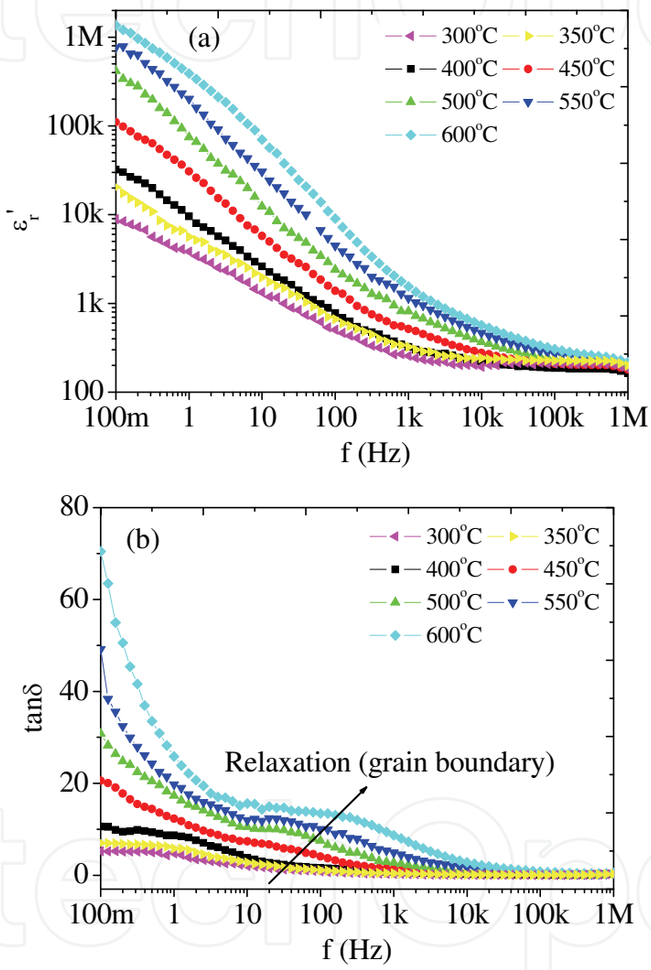

Fig. 29. The frequency dependence of (a) the dielectric constant and (b) loss at various temperatures for 8BTNTS ceramics

Fig. 29 shows the frequency dependence plots of permittivity (ε′) and dielectric loss (tanδ) at various temperatures for 8BTNTS ceramics. It is evident that at all the temperatures (Fig. 29 (a)), the value of ε′ decreases with increasing frequency and attains a constant value. The high value of the dielectric constant in low-frequency regions is a extrinsic phenomenon arising due to the presence of metallic or blocking electrodes which do not permit the mobile ions to transfer into the external circuit, and as a result, mobile ions pile up near the

electrodes and give a large bulk polarization in the materials as well as oxygen ion polarization at grain boundaries. When the temperature rises, the dispersion region shifts towards higher frequencies and the nature of the dispersion changes at low frequencies due to the electrode polarization along with grain boundary effects. A plateau region at 500 °C was observed at moderately low frequencies that shifted to higher frequencies with increase in temperature (600 °C). This plateau region distinguished electrode polarizations to the grain boundary polarizations. The variation in the tanδ with the temperature at various frequencies (Fig. 29(b)) is consistent with that of the dielectric behaviour. The loss decreases with increase in frequency at different temperatures (300-600 °C). It is also observed that the dielectric loss increases with increase in temperature which is attributed to the increase in conductivity of the ceramics due to thermal activation of conducting species. The clear relaxation peak was not encountered at any temperature under study because of dominant DC conduction losses due to high oxygen ion mobility in the temperature range under study.

5. Conclusions

We have reported the effects of composition and crystal lattice structure upon microstructure, dielectric, piezoelectric and electrical properties of BIT, $Bi_4Ti_{3-x}W_xO_{12+x}$+0.2wt%Cr_2O_3 (BTWC), $Bi_4Ti_{3-2x}Nb_xTa_xO_{12}$ (BTNT) and $Bi_4Ti_{3-2x}Nb_xTa_{x-y}Sb_yO_{12}$ (BTNTS) ceramics. WE have shown how doping can increase the piezoelectric coefficient of BIT. For the W/Cr samples, a d_{33} coefficient of 22 pC N^{-1} was measured for x=0.025. The piezoelectric coefficient d_{33} of $Bi_4Ti_{2.98}Nb_{0.01}Ta_{0.01}O_{12}$ ceramics controlled by precisely optimizing Nb/Ta amounts is found to be 26 pC N^{-1}. The highest room temperature value of the piezoelectric coefficient is found to be 35 pC N^{-1} for 8BTNTS ceramics. The antimony incorporation into the BTNT ceramics controlled electrical conductivity through reduction in the ionic and electronic conductivities as well as altered microstructure. The activation energy associated with the electrical relaxation determined from the electric modulus spectra was found to be 1.0 ± 0.03 eV, close to that of the activation energy for DC conductivity (1.08 ± 0.02 eV). It suggests that the movements of oxygen ions are responsible for both ionic conduction as well as the relaxation process. These results demonstrated that 8BTNTS ceramic is a promising candidate for high temperature piezoelectric applications.

6. References

Aurivillius, B. (1949) Mixed Bismuth Oxides with Layer Lattices: I. Structure Type of $CaBi_2B_2O_9$. *Ark. Kemi.* vol. 1, no. 54, pp. 463–480.

Ahn, C.; Jeong, E.; Kim, Y.; et al. (2009) Piezoelectric Properties of Textured $Bi_{3.25}La_{0.75}Ti_{2.97}V_{0.03}O_{12}$ Ceramics Fabricated by Reactive Templated Grain Growth Method. *J. Electroceramics*, 23, 392.

Azurmendi, N.; Caro, I.; Caballero, A.; et al. (2006) Microwave-Assisted Reaction Sintering of Bismuth Titanate–Based Ceramics. *J. Am. Ceram. Soc.*, 89, 1232.

Armstrong, R.; Newnham. E. (1972) Bismuth titanate solid solutions. *Mater. Res. Bull.* 7, 1025.

Bergman, R. (2000) General Susceptibility Functions for Relaxations in Disordered Systems. *J. Appl.Phys.* 88, 1356. 179.

Coondoo, I.; Jha A. and Agarwal S. (2007) Enhancement of dielectric characteristics in donor doped Aurivillius $SrBi_2Ta_2O_9$ ferroelectric ceramics. *J. Eur. Ceram. Soc.*, 27, 253.

Du, H.; Tang, L. & Kaskel. S. (2009) Preparation, Microstructure, and Ferroelectric Properties of $Bi_{3.25}La_{0.75}Ti_{3-x}M_xO_{12}$ (M = Mo, W, Nb, V) Ceramics. *J. Phys. Chem.C*, 113, 1329.

Ehara, S.; Muramatsu, K.; Shimazu, M.; et al. (1981) Dielectric Properties of $Bi_4Ti_3O_{12}$ Below the Curie Temperature. *Jpn. J. Appl. Phys*., 20, 877.

Fouskova, A.; Cross. L. (1970) Dielectric Properties of Bismuth Titanate. *J. Appl. Phys.* 41, 2834.

Hong, S.; Horn, J.; McKinstry, S.; et al. (2000) Dielectric and Ferroelectric Properties of Ta-doped Bismuth Titanate. J. Mater. Sci. Lett., 19, 1661.

Hong, S.; Horn, J.; McKinstry, S.; et al. (2000) Dielectric and Ferroelectric Properties of Ta-doped Bismuth Titanate. *J. Mater. Sci. Lett.*, 19, 1661.

Hou, J.; Qu, Y.; Rahul, V.; Krsmanovic, D.; Kumar. R.V. (2010) Crystallographic Evolution, Dielectric and Piezoelectric Properties of $Bi_4Ti_3O_{12}$:W/Cr Ceramics. *J. Am. Ceram. Soc.* 93, 1414.

Hou, J.; Kumar, R.V; Qu, Y.; Krsmanovic. D. (2009) B-site Doping Effect on Piezoelectric Property of $Bi_4Ti_{3-2x}Nb_xTa_xO_{12}$ Ceramics. *Scripta Materialia*, 61, 664.

Hou, J.; Rahul, V.; Qu, Kumar, R.V; (2010) Dielectric and Pyroelectric Properties of $Bi_4Ti_{2.98}Nb_{0.01}Ta_{0.01}O_{12}$ Ceramics. *Mater. Chem. Phys.* 121 , 32.

Hou, J.; Kumar, R.V.; Qu, Y.; Krsmanovic. D. Controlled synthesis of photoluminescent $Bi_4Ti_3O_{12}$ nanoparticles from metal-organic polymeric precursor. J. Nanopart. Res., 2010, 12, 563.

Hou, J.; Kumar, R.V.; Qu Y.; Krsmanovic. D. Controlled synthesis of photoluminescent $Bi_4Ti_3O_{12}$ nanoparticles from metal-organic polymeric precursor. J. Nanopart. Res., 2010, 12, 563.

Hong, S.; McKinstry, S.; Messing. G. (2000) Dielectric and Electromechanical Properties of Textured Niobium Doped Bismuth Titanate Ceramics. *J. Am. Ceram. Soc.* 83, 113.

Hou, Y.; Lu, P.; Zhu, M.; et al. (2005) Effect of Cr_2O_3 Addition on the Structure and Electrical Properties of $Pb((Zn_{1/3}Nb_{2/3})_{0.20}(Zr_{0.50}Ti_{0.50})_{0.80})O_3$ Ceramics. *Mater. Sci. Eng. B,* 116, 104.

Hyatt, N.; Reaney I. &Knight K. (2005) Ferroelectric-Paraelectric Phase Transition in the n = 2 Aurivillius Phase $Bi_3Ti_{1.5}W_{0.5}O_9$: A Neutron Powder Diffraction Study. *Phys. Rev. B*, 71, 241191.

Jardiel, T.; Caballero, A.; Villegas. M. (2006) Sintering Kinetic of $Bi_4Ti_3O_{12}$ based Ceramics. *Bol. Soc. Esp. Ceram. V*., 45, 202.

Jardiel, T.; Rubia M. & Peiteado. M. (2008) Control of Functional Microstructure in WO_3-doped $Bi_4Ti_3O_{12}$ Ceramcis. *J. Am. Ceram. Soc.*, 91, 1083.

Jardiel, T.; Villegas, M.; Caballero, A.; et al. (2008) Solid-State Compatibility in the System Bi_2O_3–TiO_2–Bi_2WO_6. *J. Am. Ceram. Soc.*, 91, 278.

Jardiel, T.; Caballero, A.; Frutos J. & Villegas. M. (2006) Sintering and Electrical Properties of $Bi_6Ti_3WO_{18}$ Ceramics. *Ferroelectrics* 336, 145.

Jonscher, A. (1977) The 'Universal' Dielectric Response. *Nature*, 267, 673.

Jaffe, B. (1971) Piezoelectric Ceramics India. Chap. 7.

Jones, J.; Slamovich, E.; Bowman, K.; et al. (2005) Domain Switching Anisotropy in Textured Bismuth Titanate Ceramics. *J. Appl. Phys.*, 98, 104102.

Kohlrausch, R. (1954) Theorie Des Elektrischen Rückstandes in Der Leidner Flasche. *Prog. Ann. Phys.*, 91,

Li, J. & Sun. Q. (2008) Effects of Cr_2O_3 Doping on the Electrical Properties and the Temperature Stabilities of PZT Binary Piezoelectric Ceramics. *Rare Metals*, 27, 362.

Kumar, M. & Ye. Z. (2001) Dielectric and electric properties of the donor- and acceptor-doped ferroelectric $SrBi_2Ta_2O_9$. *J. Appl. Phys.* 90, 934.

Kan, Y.; Jin, X.; Zhang, G.; et al. (2004) Lanthanum Modified Bismuth Titanate Prepared by a Hydrolysis Method. *J. Mater. Chem.*, 14, 3566.

Lopatin, S. (1989) Translated from Izvestiya Akademii Nauk SSSR, Neorganicheskie Materialy 24, 1551.

Luo, S.; Noguchi, Y.; Miyayama M. & Kudo. T. (2001) Rietveld Analysis and Dielectric Properties of Bi_2WO_6-$Bi_4Ti_3O_{12}$ Ferroelectric System. *Mater. Res. Bull.*, 36, 531.

Luo, S.; Noguchi, Y.; Miyayama M. & Kudo. T. (2001) Rietveld Analysis and Dielectric Properties of Bi_2WO_6-$Bi_4Ti_3O_{12}$ Ferroelectric System. *Mater. Res. Bull.*, 36, 531.

Macedo, P.; Moynihan, C.; Bose. R. (1972) Role of Ionic Diffusion in Polarization in Vitreous Ionic Conductors. P*hys. Chem. Glasses*, 13, 171.

Markovec, D.; Pribošic, I.; Samardžija, Z.; Drofenik. M. (2001) Incorporation of Aliovalent Dopants into the Bismuth-Layered Perovskite-Like Structure of $BaBi_4Ti_4O_{15}$. *J. Am. Ceram. Soc.* 84, 2702.

Noguchi, Y.; Miwa, I.; Goshima, Y.; et al. (2000) Oxygen-vacancy-induced 90°-domain clamping in ferroelectric $Bi_4Ti_3O_{12}$ single crystals. *Jpn. J. Appl. Phys.* 39, L1259.

Nagata, H. (2004) Ceramic Transactions. Ceramic Materials and Multilayer Electronic Devices. *J. Am. Ceram. Soc.*, 150.

Nagata, H.; Chikushi, N.; Takenaka T. (1999) Piezoelectric Properties of Bismuth Layer-Structured Ferroelectric Ceramics with Sr-Bi-Ti-Ta System. *Jpn. J. Appl. Phys.* 38, 5497.

Ngai, K.; Rendell, R.; Jain. H. (1984) Anomalous Isotope-mass Effect in Lithium Borate Glasses: Comparison with a Unified Relaxation Model. *Phys. Rev. B*, 30, 2133.

Peiteado, M.; Rubia, M.; Fernandez, J.; et al. (2006) Thermal Evolution of ZnO-Bi_2O_3 -Sb_2O_3 System in the Region of Interest for Varistor. *J. Mater. Sci.*, 41, 2319.

Rojero, M.; Romero, J.; Marcos, F.; et al. (2010) Intermediate Phases Formation During the Synthesis of $Bi_4Ti_3O_{12}$ by Solid State Reaction. *Ceram. Int.*, 36, 1319.

Shulman, H.; Damjanovic, D.; Setter. N. (2000) Niobium Doping and Dielectric Anomalies in Bismuth

Titanate. *J. Am. Ceram. Soc.* 83, 528.

Shulman, H.; Testorf, M.; Damjanovic, D.; Setter. N. (1996) Microstructure, Electrical Conductivity, and Piezoelectric Properties of Bismuth Titanate. J. Am. Ceram. Soc. 79, 3124.

Shimazu, M.; Tanaka, J.; Muramatsu, K.; et al. (1980) Phase transition in the family $La_xBi_{4-x}Ti_3O_{12}$: In relation to lattice symmetry and distortion. *J. Solid State Chem.* 35, 402.

Sugibuchi, K.; Kurogi, Y.; Endo. N. (1975) Ferroelectric field-effect memory device using $Bi_4Ti_3O_{12}$ film. *J. Appl. Phys.* 47, 2877.

Snyder, R.; Fiala, J. &Bunge. J. (1999) Defect and Microstructure Analysis by Diffraction. International Union of Crystallography, Oxford Science Publication, Oxford.

Subbarao, E. (1961). Ferroelectricity in $Bi_4Ti_3O_{12}$ and Its Solid Solutions. *Phys. Rev.* 122, 804.

Saito, Y.; Takao, H.; Tani, T.; et al. (2004) Lead-free piezoceramics. *Nature*, 432, 84.

Shimakawa, Y.; Kubo, Y.; Tauchi, Y.; et al. (2000) Structural distortion and ferroelectric properties of $SrBi_2(Ta_{1-x}Nb_x)_2O_9$. Appl. Phys. Lett. 77, 2749.

Takahashi, M.; Noguchi, Y. & Miyayama. M. (2003) Effects of V-Doping on Mixed Conduction Properties of Bismuth Titanate Single Crystals. *Jpn. J. Appl. Phys*., 42, 6222.

Takahashi, M.; Noguchi, Y.; Miyayama. M. (2004) Estimation of Ionic and Hole Conductivity in

Bismuth Titanate Polycrystals at High Temperatures. *Solid State Ionics*, 172, 325.

Takahashi, M. (1970) Space Charge Effect in Lead Zirconate Titanate Ceramics Caused by the Addition of Impurities. *Japan J. Appl. Phys*., 9, 1236.

Tang, Q.; Kan, Y.; Li, Y.; et al. (2006) Effect of Vanadium Doping on Fabrication and Property of $Bi_4Ti_3O_{12}$ Ceramics. *Scripta Materialia*, 54, 2075.

Tang, Q.; Kan, Y.; Li, Y.; et al. (2007) Ferroelectric and Dielectric Properties of Nd/V Co-doped $Bi_4Ti_3O_{12}$ Ceramics. *Solid State Commun*.,142, 1.

Takenaka, T. & Sakata. K. (1981) Electrical properties of grain-oriented ferroelectric ceramics in some lanthanum modified layer-structure oxides. *Ferroelectrics.* 38, 769.

Uchino, K. (2000) Ferroelectric Devices, New York. Chap. 7.

Villegas, M.; Caballero, A.; Moure, C.; et al. (1999) Factors Affecting the Electrical Conductivity of Donor-Doped $Bi_4Ti_3O_{12}$ Piezoelectric Ceramics. *J. Am. Ceram. Soc.* 82, 2411.

Villegas, M.; Caballero, A.; Moure, C.; et al. (1999) Low-temperature sintering and electrical properties of chemically W-doped $Bi_4Ti_3O_{12}$ ceramics. *J. Eur. Ceram. Soc.* 19, 1183.

Villegas, M.; Jardiel, T & Farias. G. (2004) Sintering and Electrical Properties of $Bi_4Ti_{2.95}W_xO_{11.9+3x}$ piezoelectric ceramics. *J. Eur. Ceram. Soc.,* 24, 1025.

Vaish, R.; Varma. K. (2009) Dielectric Properties of Li_2O-$3B_2O_3$ Glasses. *J. Appl. Phys.,* 106, 064106.

Vaish, R.; Varma. K. (2009) Low Loss and Frequency (1 kHz-1 MHz) Independent Dielectric Characteristics of 3BaO-$3TiO_2$-B_2O_3 Glasses. *J. Appl. Phys.,* 106, 114109.

Williams G. & Watts. D. (1970) Non-Symmetrical Dielectric Relaxation Behaviour Arising from a Simple Empirical Decay Function. *Trans. Faraday Soc*., 66, 80.

Yang, Z.; Zhang, R.; Yang, L.; et al. (2007) Effects of Cr_2O_3 Doping on the Electrical Properties and the Temperature Stabilities of PNW–PMN–PZT Ceramics. *Mater. Res. Bull*., 42, 2156.

Zhang, H.; Yan H. and Reece. M. (2009) The Effect of Nd Substitution on the Electrical Properties of Bi_3NbTiO_9 Aurivillius Phase Ceramics. *J. Appl. Phys*., 106, 044106.

Zhao, P. & Zhang. B. (2008) High Piezoelectric d_{33} Coefficient in Li/Ta/Sb-Codoped Lead-Free (Na,K)NbO_3 Ceramics Sintered at Optimal Temperature. *J. Am. Ceram. Soc*., 91, 3078.

Zhang, L.; Zhao, S.; Yu, H.; et al. (2004) Microstructure and Electrical Properties of Tungsten-Doped Bismuth Titanate Ceramics. *Jap. J. Appl. Phy*., 43, 7613.

Zhang, L.; Chu, R.; Zhao, S.; et al. (2005) Microstructure and Electrical Properties of Niobium Doped $Bi_4Ti_3O_{12}$ Layer-structured Piezoelectric Ceramics. *Mater. Sci. Eng. B*, 116, 99.

Zhou, Z.; Dong, X.; Yan, H.; et al. (2006) Doping Effects on the Electrical Condcutivity of Bismuth Layered Bi_3TiNbO_9-based Ceramics. *J. Appl. Phys*., 100, 044112.

Zhang, Q.; Zhang, B.; Li, H.; et al. (2010) Effects of Sb content on electrical properties of lead-free piezoelectric $[(Na_{0.535}K_{0.480})_{0.942}Li_{0.058}](Nb_{1-x}Sb_x)O_3$ ceramics *J. Ally. Compd*., 490, 260.

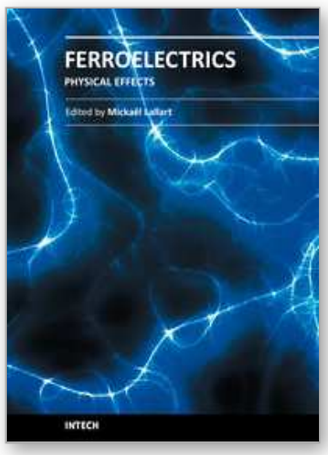

Ferroelectrics - Physical Effects

Edited by Dr. MickaÃ«l Lallart

ISBN 978-953-307-453-5
Hard cover, 654 pages
Publisher InTech
Published online 23, August, 2011
Published in print edition August, 2011

Ferroelectric materials have been and still are widely used in many applications, that have moved from sonar towards breakthrough technologies such as memories or optical devices. This book is a part of a four volume collection (covering material aspects, physical effects, characterization and modeling, and applications) and focuses on the underlying mechanisms of ferroelectric materials, including general ferroelectric effect, piezoelectricity, optical properties, and multiferroic and magnetoelectric devices. The aim of this book is to provide an up-to-date review of recent scientific findings and recent advances in the field of ferroelectric systems, allowing a deep understanding of the physical aspect of ferroelectricity.

InTech Europe
University Campus STeP Ri
Slavka Krautzeka 83/A
51000 Rijeka, Croatia
Phone: +385 (51) 770 447
Fax: +385 (51) 686 166
www.intechopen.com

InTech China
Unit 405, Office Block, Hotel Equatorial Shanghai
No.65, Yan An Road (West), Shanghai, 200040, China
中国上海市延安西路65号上海国际贵都大饭店办公楼405单元
Phone: +86-21-62489820
Fax: +86-21-62489821

IntechOpen